# Internet data centers and industrial parks as flexibility providers in modern power systems An ADMM-based coordination mechanism

Mansouri, Seyed Amir; Nematbakhsh, Emad; Ramos, Andrés; Chaves-Avila, Jose Pablo; García-González, Javier; Aguado, José A.

**DOI**
10.1016/j.apenergy.2025.127320

**Licence**
CC BY

**Publication date**
2026

**Document Version**
Final published version

**Published in**
Applied Energy

**Citation (APA)**
Mansouri, S. A., Nematbakhsh, E., Ramos, A., Chaves-Avila, J. P., García-González, J., & Aguado, J. A. (2026). Internet data centers and industrial parks as flexibility providers in modern power systems: An ADMM-based coordination mechanism. *Applied Energy*, *407*, Article 127320. https://doi.org/10.1016/j.apenergy.2025.127320

Applied Energy 407 (2026) 127320

Contents lists available at ScienceDirect

Applied Energy

journal homepage: www.elsevier.com/locate/apenergy

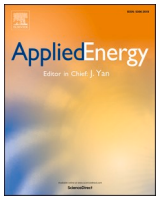

# Internet data centers and industrial parks as flexibility providers in modern power systems: An ADMM-based coordination mechanism

Seyed Amir Mansouri [a,b,*], Emad Nematbakhsh [b], Andrés Ramos [b], Jose Pablo Chaves-Avila [b], Javier García-González [b], José A. Aguado [c]

[a] Department of Engineering Systems & Services, Faculty of Technology, Policy & Management, Delft University of Technology, Delft, the Netherlands
[b] Institute for Research in Technology (IIT), ICAI School of Engineering, Comillas Pontifical University, 28015 Madrid, Spain
[c] Department of Electrical Engineering, Escuela de Ingenierías Industriales, University of Málaga, 29010 Málaga, Spain

## HIGHLIGHTS

- Bi-level mechanism maximizes flexibility services from smart prosumers.
- Proxy-driven algorithm enables geo-distributed IDC service-sharing across zones.
- Adaptive ADMM accelerates convergence by 74.5 % with minimal data exchange.
- Case study shows 35.2 % lower congestion costs and higher prosumer revenues.

## ARTICLE INFO

*Keywords:*
Industrial parks
Internet data Centers
Congestion management
Distributed optimization
Smart prosumers
Smart grids

## ABSTRACT

Smart prosumers with Distributed Generation (DGs) and controllable loads can provide cost-effective grid services. However, realizing this potential requires distributed optimization mechanisms that ensure market efficiency, participant privacy, and compliance with electricity market regulations. This paper presents a bi-level distributed optimization mechanism to maximize flexibility services from industrial parks and Internet Data Centers (IDCs) in distribution-level Congestion Management (CM) markets. The upper-level models the Distribution System Operator (DSO), which identifies congested lines using linear AC power flow analysis on pre-settled energy market results and sends corrective signals to prosumers. The lower level allows prosumers to adjust their operations accordingly and communicate updated transactions back to the DSO. A novel proxy-driven algorithm is proposed to facilitate service-sharing among geo-distributed IDCs, considering congestion issues. Additionally, an adaptive Alternating Direction Method of Multipliers (ADMM) algorithm enables decentralized coordination among market agents, achieving 74.52 % faster convergence than the standard ADMM. A real-world case study from Spain demonstrates that the proposed mechanism enables the grid operator to maximize grid services from prosumers, reducing congestion alleviation costs by 35.27 %. Moreover, IDCs reduced daily costs by 11.07 % through service-sharing and task-shifting aligned with CM market signals, while industrial parks achieved a 13.68 % cost reduction by aligning material production processes with CM market signals, both enabled by the proposed bi-level mechanism.

## 1. Introduction

### 1.1. Background and motivation

The integration of Distributed Energy Resources (DERs) and advancements in smart grid technologies have redefined power system operations, creating opportunities for decentralized grid services [1,2]. Industrial parks and IDCs are emerging as key smart prosumers, equipped with generation units, energy storage systems, and controllable loads [3,4]. These entities hold the potential to provide essential grid services, including congestion alleviation, frequency regulation, and load balancing, which are vital for maintaining grid reliability and efficiency [5,6]. Conventional centralized grid management approaches

* Corresponding author at: Department of Engineering Systems & Services, Faculty of Technology, Policy & Management, Delft University of Technology, Delft, the Netherlands
*E-mail addresses:* s.mansouri@tudelft.nl, amir.mansouri24@gmail.com (S.A. Mansouri).

https://doi.org/10.1016/j.apenergy.2025.127320
Received 20 September 2025; Received in revised form 20 November 2025; Accepted 24 December 2025
Available online 2 January 2026

**Nomenclature**

*Abbreviations*

| | |
|---|---|
| ADMM | Alternating Direction Method of Multipliers |
| CHP | Combined Heat and Power |
| CM | Congestion Management |
| DER | Distributed Energy Resources |
| DG | Distributed Generation |
| DLC | Direct Load Control |
| DSO | Distribution System Operator |
| HDD | Hard Disk Drive |
| IDC | Internet Data Center |
| MILP | Mixed-Integer Linear Programming |
| MIQCP | Mixed-Integer Quadratically Constrained Programming |
| PTDF | Power Transfer Distribution Factor |
| PV | Photovoltaic |

*Sets*

| | |
|---|---|
| $c$ | Index of IDC's clusters |
| $d$ | Index of IDCs |
| $es$ | Index of grid-connected storage systems |
| $g$ | Index of controllable generations |
| $i, j$ | Index of distribution buses |
| $m$ | Index of materials |
| $n$ | Index of industrial parks |
| $pv$ | Index of PV units |
| $s$ | Index of IDC's services |
| $t$ | Index of time periods |
| $x$ | Index of piecewise segments |

*Scalars*

| | |
|---|---|
| $\alpha/\beta$ | Multiplicative / Division factor |
| $C^p$ | Specific heat capacity of air (kJ/kg.°C) |
| $\Delta t$ $\Delta t$ | Time step (h) |
| $\delta^{min}/\delta^{max}$ | Min/Max voltage angle (rad) |
| $\eta^{PV}$ | Efficiency of PV panels (%) |
| $\eta^{Ch}/\eta^{Dis}$ | Efficiency of charging/discharging process (%) |
| $IR^{STC}$ | Sun irradiance at standard test conditions (W/m$^2$) |
| $\lambda^{ES}$ | Operation cost of storage systems ($/kWh) |
| $\lambda^{DLC}$ | Cost of applying DLC ($/kWh) |
| $M$ | Big positive number |
| $\rho$ | Air density (kg/m$^3$) |
| $S^{Base}$ | Base power (kVA) |
| $V^{min}/V^{max}$ | Min/Max voltage magnitude (p.u) |

*Parameters*

| | |
|---|---|
| $A_d/B_d$ | Power consumption coefficients (kW/GHz$^3$ - kW) |
| $CM_d$ | Capacity margin of IDCs (tasks/h) |
| $D_{s,c,d}$ | Server response time (h) |
| $E_{es}^{ES,In}$ | Initial energy level of grid-connected storage systems (kWh) |
| $E_n^{(.),In}$ | Initial material storage level in industrial parks (units) |
| $E_{es}^{ES,min}/E_{es}^{ES,max}$ | Min/Max energy level of grid-connected storage systems (kWh) |
| $E_n^{(.),min}/E_n^{(.),max}$ | Min/Max material storage level in industrial parks (units) |
| $\varepsilon$ | Inertia coefficient |
| $\eta_d^{AC}$ | Cooling system efficiency (%) |
| $\eta_n^{B,gh}$ | Boiler conversion factors (kWh/m$^3$) |
| $\eta_n^{CHP,ge}/\eta_n^{CHP,gh}$ | CHP conversion factors (kWh/m$^3$) |
| $F_{s,c,d,x}^{IDC}$ | CPU frequencies (GHz) |
| $G_l/B_l/R_l$ | Conductance/Susceptance/Resistance of branches (p.u) |
| $G_{n,t}^{IP,EM}$ | Gas consumption of industrial parks in the energy market (m$^3$/h) |
| $\gamma_i/\gamma_d/\gamma_n$ | Reactive power rates (kVAR/kW) |
| $H_n^{B,max}$ | Boiler capacity (kW) |
| $IR_t$ | Sun irradiance (W/m$^2$) |
| $\lambda_t^{Proxy}$ | Operation cost of proxy ($/tasks) |
| $\lambda_t^{Gas}$ | Gas price ($/m$^3$) |
| $\lambda_{n,t}^{CM}/\lambda_{d,t}^{CM}$ | Congestion management prices ($/kWh) |
| $\varphi_t^{EM}$ | Penalty for adjusting power exchanges with the upstream grid ($/kWh) |
| $\varphi_t^{CG}$ | Penalty for adjusting power exchanges with controllable generation ($/kWh) |
| $\varphi_{pv}$ | Max reactive power capacity of PV unit (%) |
| $M_{n,t}^{min,(.)}/M_{n,t}^{max,(.)}$ | Min/Max material production level (units/h) |
| $M_{n,t}^{Prod,Desire}$ | Desired final material production curve (units/h) |
| $P_d^{AC,min}/P_d^{AC,max}$ | Min/Max power consumption of IDC's air-conditioning system (kW) |
| $P_{s,c,d}^{IDC,min}/P_{s,c,d}^{IDC,max}$ | Min/Max power consumption of clusters in each service (kW) |
| $P_{es}^{Ch,max}/P_{es}^{Dis,max}$ | Max charging/discharging capacity of grid-connected storage systems (kW) |
| $P_{pv}^{Rate}$ | Rated capacity of PV units (kW) |
| $P_t^{UG,EM}$ | Power exchange with upstream grid in the energy market (kW) |
| $P_{g,t}^{CG,EM}$ | Power exchange with controllable generations in the energy market (kW) |
| $P_{n,t}^{IP,EM}$ | Power exchange of industrial parks in the energy market (kW) |
| $P_{d,t}^{IDC,EM}$ | Power exchange of IDCs in the energy market (kW) |
| $P_g^{CG,min}/P_g^{CG,max}$ | Min/Max active power capacity of controllable generation (kW) |
| $P_{i,t}^D/Q_{i,t}^D$ | Active/Reactive load demands (kW - kVAR) |
| $P_n^{(.)}/h_n^{(.)}$ | Edging power/Heating operation points of CHP units (kW) |
| $P_{n,t}^{PV}$ | Power generation by PV unit in industrial parks (kW) |
| $P_{n,t}^{Fixed}/H_{n,t}^{Fixed}$ | Fixed power/heating load demands of industrial parks (kW) |
| $Q_g^{CG,min}/Q_g^{CG,max}$ | Min/Max reactive power capacity of controllable generation (kW) |
| $\rho^{IDC}/\rho^{IP}$ | Penalty Parameters |
| $r^{P,IDC/IP}/r^{D,IDC/IP}$ | Primal/Dual residuals |
| $\sigma_{s,c,d,x}^{IDC}$ | Fractional segments of server capacity (tasks/h) |
| $S_l^{Line,max}$ | Branch capacity (kW) |
| $\theta_d^{min}/\theta_d^{max}$ | Min/Max allowable temperature for air-conditioning system (°C) |
| $U_{s,c,d}^{max}$ | Maximum utilization rate (%) |
| $\upsilon_i$ | Max DLC level (%) |
| $\omega_{i,l}$ | Flow direction |
| $\varpi_d^{IDC}$ | Predefined computing service requirements (h) |
| $\omega_{s,c,d,t}^{IDC}$ | Workload before service sharing (tasks/h) |
| $W^{H,(.)}/W^{G,(.)}/W^{P,(.)}$ | Weighting factors for the material production process (units/kWh – units/m$^3$ - units/kWh) |
| $\psi_d$ | Airflow rate (m$^3$/s) |
| $\chi_{s,c,d}^{IDC,min}/\chi_{s,c,d}^{IDC,max}$ | Min/Max capacity of clusters (tasks/h) |

*Variables*

| | |
|---|---|
| $\delta_{i,t}$ | Voltage angle (rad) |
| $e_{es,t}^{ES}$ | Energy level of grid-connected storage systems (kWh) |
| $e_{n,t}^{(.)}$ | Material storage level in industrial parks (units) |
| $\theta_{d,t}^{Indoor}$ | Indoor temperature of IDCs (°C) |
| $\theta_{d,t}^{Output}$ | Output temperature of air-conditioning system (°C) |

| | |
|---|---|
| $f^{IDC}_{s,c,d,t}$ | CPU frequency (GHz) |
| $g^{IP}_{n,t}$ | Total gas consumption of the industrial park ($m^3$/h) |
| $g^{B}_{n,t}$ | Gas consumption of boiler ($m^3$/h) |
| $g^{CHP}_{n,t}$ | Gas consumption of CHP ($m^3$/h) |
| $g^{(T1-T6)}_{n,t}$ | Gas consumption in the material production process ($m^3$/h) |
| $h^{B}_{n,t}$ | Heat generated by boiler (kW) |
| $h^{(T1-T6)}_{n,t}$ | Heat consumption in the material production process (kW) |
| $m^{Prod,(.)}_{n,t}$ | Material produced in production lines of industrial parks (units/h) |
| $m^{Used,(.)}_{n,t}$ | Material used in production lines of industrial parks (units/h) |
| $p^{AC}_{d,t}$ | Power consumption of the air-conditioning system (kW) |
| $p^{IDC}_{d,t}/\widetilde{p}^{IDC}_{d,t}$ | Coupling variables representing the power exchange of IDCs (kW) |
| $p^{IDC}_{s,c,d,t}$ | Power consumption of different clusters in each service (kW) |
| $p^{IP}_{n,t}/\widetilde{p}^{IP}_{n,t}$ | Coupling variables representing the power exchange of industrial parks (kW) |
| $p^{IP,Buy}_{n,t}/p^{IP,Sell}_{n,t}$ | Buying/Selling power by industrial parks (kW) |
| $p^{Line}_{l,t}/q^{Line}_{l,t}$ | Active/Reactive power flow (kW - kVAR) |
| $p^{PV}_{pv,t}/q^{PV}_{pv,t}$ | Active/Reactive power generated by grid-connected PV units (kW - kVAR) |
| $p^{(.)\to(.)}_{n,t}/h^{(.)\to(.)}_{n,t}$ | Internal power/heat flow in industrial parks (kW) |
| $p^{ES,Ch}_{n,t}/h^{TS,Ch}_{n,t}$ | Charging level of electrical/thermal storage systems (kW) |
| $p^{ES,Dis}_{n,t}/h^{TS,Dis}_{n,t}$ | Discharging level of electrical/thermal storage systems (kW) |
| $p^{DLC}_{i,t}$ | Power curtailed via DLC (kW) |
| $p^{CG}_{g,t}/q^{CG}_{g,t}$ | Active/Reactive power generated by grid-connected controllable generations (kW - kVAR) |
| $p^{UG}_{t}/q^{UG}_{t}$ | Active/Reactive power exchange with upstream grid (kW - kVAR) |
| $p^{Ch}_{es,t}/p^{Dis}_{es,t}$ | Charging/Discharging power of grid-connected storage systems (kW) |
| $p^{Loss}_{l,t}$ | Power losses (kW) |
| $p^{CHP}_{n,t}/h^{CHP}_{n,t}$ | Power/Heat operating points of CHPs |
| $p^{(T1-T6)}_{n,t}$ | Power consumption by material production process (kW) |
| $u_{s,c,d,t}$ | Utilization rate (%) |
| $v_{i,t}$ | Voltage magnitude (p.u.) |
| $\omega^{Proxy,In}_{s,c,d,t}/\omega^{Proxy,Out}_{s,c,d,t}$ | Incoming/Outgoing services of IDCs (tasks/h) |
| $\chi^{IDC}_{s,c,d,t}$ | Task quantity of different clusters in each service (tasks/h) |
| $z^{IDC}_{s,c,d,t}$ | Modulation factor of computing services (h) |

*Binary variables*

| | |
|---|---|
| $i^{AC}_{d,t}$ | Flag status of the air-conditioning system at the minimum temperature |
| $o^{AC}_{d,t}$ | Flag status of the air-conditioning system at the maximum temperature |
| $i^{Freq}_{s,c,d,x,t}$ | Status of piecewise segments |
| $i^{Ch}_{es,t}/i^{Dis}_{es,t}$ | Charging/Discharging status of grid-connected storage systems |
| $i^{IDC}_{s,c,d,t}$ | Status of IDC clusters in each service |
| $i^{CHP}_{n,t}$ | Status of CHP |

struggle to scale effectively in modern power systems, particularly with the growing number of prosumers and DERs [7,8]. Centralized systems also pose challenges regarding data privacy, communication bottlenecks, and regulatory compliance. As a result, there is an increasing demand for decentralized optimization mechanisms that can securely and efficiently coordinate grid services from prosumers without compromising operational data privacy or market regulations [9–11].

The motivation behind this work is to harness the untapped potential of industrial parks and IDCs to provide cost-effective grid services within local CM markets. To achieve this, the paper proposes an adaptive ADMM-based distributed coordination mechanism that enables the DSO to efficiently coordinate these decentralized smart prosumers while preserving their data privacy.

### 1.2. Literature review

Significant prior research has focused on deriving grid services from smart prosumers and DERs in local CM markets. In this context, models presented in [12,13] address CM services provided by DERs within microgrids, [14,15] focus on extracting these services from local resources within energy communities, and [16] highlight the provision of CM services from energy hubs. However, there is limited research on leveraging CM services from industrial parks and IDCs. Studies [17–19] have explored the optimal participation of industrial parks in energy markets, with [17,18] considering energy flows between DERs within industrial parks, albeit with simplified production line models. These studies employed centralized optimization approaches that did not account for privacy in the market participation of industrial parks. Conversely, [19] introduced a hierarchical structure that facilitated the participation of industrial parks in energy markets with limited information sharing, while accurately modelling both the energy flow among DERs and the production lines of the industrial parks. Similarly, [20] employed a hierarchical optimization structure with limited information sharing to assess the potential of industrial parks to provide CM services, though the production line model was simplified.

The involvement of IDCs as smart prosumers with time-shiftable loads in energy markets has been assessed in [21–26]. The authors in [22–25] employed centralized optimization structures to integrate IDCs into energy markets, while a hierarchical optimization approach was utilized in [21]. In [21,22,26], IDCs can share some of their services with other centers within a common area, while [23–25] present more realistic models that enable service sharing between geographically distributed data centers. Only [26] evaluated the potential of IDCs to provide CM services, employing an adaptive ADMM algorithm to integrate them into the local CM market. However, this study did not explore the potential of service sharing between geographically distributed IDCs operating across different time zones.

Recent research on organizing local CM markets with high participation from smart prosumers has employed various power flow models to identify potential congestion within networks. The authors in [14] employed a nonlinear AC power flow model, [12,16,27–29] used linear AC models, [13,21,30] adopted DC models, and [31] applied Power Transfer Distribution Factors (PTDFs), all aimed at identifying congested lines. However, most of these models were tested on benchmark test systems, with only [21] validating their approach through implementation on a real-world case study involving an 11-zone aggregation of the New York power system. In [16,18,22–25,31], centralized optimization structures are employed to coordinate smart prosumers with the market operator, compromising prosumer privacy. Hierarchical optimization techniques are utilized in [15,19–21] for this coordination, preserving privacy but failing to achieve the global optimal solution in market optimization. In contrast, distributed optimization techniques are applied in [12–14,17,26–30] for coordinating smart prosumers with market operators, using ADMM algorithms in [12,14,17,26,27,29], an

**Table 1**
Comparative analysis of proposed and recent Models.

| Industrial Parks | | | |
|---|---|---|---|
| Internal Converters | | Production Line | CM Market |
| [17]– [18] - [19]– [20] * | | [19] - * | [20]* |
| **Internet Data Centers** | | | |
| Internal Devices | | Proxy-Driven Service Sharing Across Geo-Distributed, Multi-Time-Zone IDCs | CM Market |
| [21]– [22] - [24]– [25] - [26] - * | | [24]– [25] - * | [26] - * |
| **Optimization Framework** | Centralized | [16]– [18] - [22]– [23] - [24]– [25] - [31] | |
| | Distributed | [12]– [13] - [14]– [17]- [26]– [27] | |
| | Hierarchical | [28]– [29] - [30] - * | |
| **Multi-Level Market Modelling for Industrial Parks / IDCs** | | [15]– [19]– [20]– [21] | |
| **ADMM-Based Market Coordination for Industrial Parks / IDCs** | | [17]– [19]– [20]– [21] - [26] - * | |
| **Improved and Accelerated ADMM Variants** | | [17]– [26] - * | |
| **Market Coordination with Minimal Data Exchange for Industrial Parks / IDCs** | | [29] - * | |

alternating iterative method in [13], a Stackelberg game theory in [28], and a step-wise procedure in [30]. These studies demonstrate that distributed optimization techniques can simultaneously preserve prosumer privacy and achieve the global optimal solution.

### 1.3. Research gap and contributions

In Table 1, the proposed model, denoted by an asterisk (*), is compared against other models from recent literature. The review highlights that very few studies have focused on the extraction of CM services from industrial parks and IDCs. Most works have either addressed the optimal scheduling of these smart prosumers individually or their participation in energy markets, often neglecting their potential to provide grid services. To the authors' knowledge, only [20,26] have evaluated the capability of industrial parks and IDCs to offer grid services to CM markets. However, these studies have not simultaneously considered both industrial parks and IDCs, failed to accurately model industrial parks' production lines, and overlooked the potential for service-sharing between geo-distributed IDCs. This creates a significant research gap that requires a detailed assessment of the capacity of industrial parks and IDCs to provide grid services. Consequently, it is crucial to develop distributed optimization structures that ensure a secure and optimal environment for the participation of all decentralized parties in the market. While [12–14,17,26–30] have demonstrated that distributed optimization methods can be effective and secure for electricity market optimization, they are challenged by long convergence times, a critical issue that still needs to be addressed.

To address these gaps, this paper proposes an adaptive ADMM-based distributed coordination mechanism that enables the DSO, acting as market organizer, to efficiently coordinate smart prosumers, specifically, industrial parks and IDCs, in local CM markets. The proposed framework integrates detailed techno-economic models of industrial parks and IDCs, capturing their respective flexibility mechanisms: production chain rescheduling and energy management for industrial parks, and service shifting and proxy-based service sharing for IDCs. The main contributions of this study are as follows:

- A bi-level mechanism is introduced for distributed optimization of decentralized smart prosumers, particularly industrial parks and IDCs, within local CM markets. This mechanism incorporates congestion management at the upper level and smart prosumers' scheduling at the lower level, enabling an iterative exchange of optimization signals between the two levels. It allows industrial parks and IDCs to adjust their material production and service-sharing activities, respectively, in response to grid service requirements communicated by the system operator.
- A novel proxy-driven algorithm for service-sharing among geo-distributed IDCs is presented, enabling them to offload part of their tasks to centers in other time zones during congested periods and receive services during non-congested periods. This method leverages time zone differences to optimize resource utilization and enhance IDCs' flexibility. An adaptive ADMM algorithm is also introduced for distributed optimization between smart prosumers and the DSO in local CM markets, ensuring convergence to the global optimum with minimal data exchange. By dynamically adjusting penalty parameters, the adaptive ADMM remarkably accelerates convergence compared to the standard version.
- The proposed mechanism maximizes the provision of grid services from industrial parks and IDCs to mitigate congestion in local markets, reducing the system operator's reliance on controllable fossil-fueled units. In addition to generating significant daily revenue for smart prosumers, the approach significantly lowers congestion alleviation costs for the system operator.

### 1.4. Organization

The remainder of this paper is structured as follows. Section 2 introduces the proposed framework and its main components. Section 3 details the mathematical formulation of the DSO, IDC, and industrial park models, together with the adaptive ADMM-based coordination.

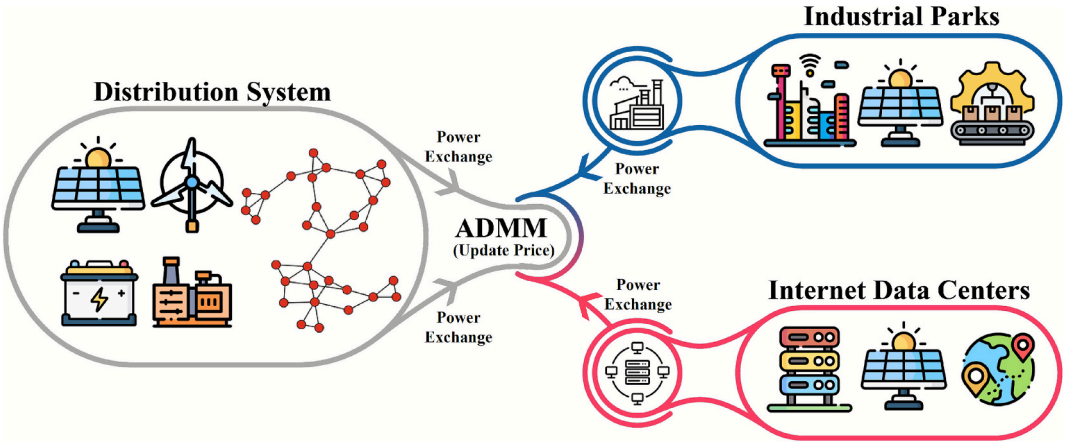


**Fig. 1.** The outline of the proposed bi-level mechanism.

Section 4 presents the implementation workflow, while Section 5 reports the case study results and performance analysis. Section 6 concludes the paper and outlines future research directions.

## 2. Model outline

The framework proposed in this paper aligns with the objectives of the Spanish national project OptiREC [32], which aims to design decentralized local CM markets for distribution networks, as such markets are not yet established in Spain. The proposed framework enables the DSO, acting as the market organizer, to efficiently coordinate smart prosumers, including industrial parks and IDCs, in providing flexibility services to alleviate local congestion. In this framework, the DSO, which has the capability to run power flow programs in the distribution system, acts as the market organizer, while decentralized smart prosumers serve as active participants. The local CM market operates a few hours after the day-ahead energy market and one day prior to real-time operations. Fig. 1 illustrates the outline of the proposed bi-level mechanism. At the upper level, the DSO identifies and mitigates congestion in its service area using a linear AC power flow model. The DSO seeks to alleviate congestion by making minimal adjustments to nodal production and consumption relative to the pre-established energy market outcomes. The DSO's congestion management strategies include adjusting generation or consumption at nodes linked to subscribers with Direct Load Control (DLC) contracts, controllable generation units, energy storage systems, and smart prosumers. Once these adjustments are determined, the DSO sends power exchange correction signals to the smart prosumers.

At the lower level, smart prosumers adjust the schedules initially submitted to the day-ahead energy market in response to signals from the DSO, aiming to maximize their profits in the local CM market. Industrial parks can optimize the operation of their DERs, such as Combined Heat and Power (CHP) systems, boilers, and thermal and electric storage systems, or shift part of their material production to non-congested periods. Data centers can shift part of their interruptible services to less congested times or transfer non-interruptible services to centers in different time zones via proxies. After these adjustments, smart prosumers communicate their updated power exchanges to the DSO.

An adaptive version of the ADMM is developed to enable signal exchanges between the upper and lower levels within a decentralized framework. This version follows the standard ADMM process, iteratively exchanging coupling variables (i.e., power exchange signals between prosumers and the DSO) during the optimization process until global convergence is achieved. It ensures the privacy of all market agents through minimal information sharing. In the proposed version, the ADMM algorithm's penalty term is dynamically updated at each iteration based on the behavior of market agents, significantly improving the convergence speed.

## 3. Mathematical modelling

The proposed bi-level mechanism is formulated as a Mixed-Integer Linear Programming (MILP) problem, but with the application of an adaptive ADMM using a 2-norm penalty term, it is transformed into a Mixed-Integer Quadratically Constrained Programming (MIQCP) problem. In this formulation, indices *n*, *d*, *g*, *pv*, and *es* represent industrial parks, IDCs, controllable generation units, Photovoltaic (PV) units, and grid-connected storage systems, respectively. Indices *s* and *c* correspond to services and clusters within IDCs, while index *m* represents materials within industrial parks. Variables related to the energy market, already determined and provided to the DSO, are denoted with superscript *EM*. It should be stated that parameters are represented by uppercase letters, while variables are in lowercase.

### 3.1. Upper level (DSO scheduling)

Eq. (1) defines the objective function of the DSO, who acts as the market organizer in the local CM market. The DSO's goal is to mitigate network congestion while ensuring that deviations from the pre-established energy market schedules remain minimal. This objective represents the DSO's practical task of maintaining secure and efficient network operation with the lowest possible cost. The first and second terms in (1) quantify the costs of adjusting power exchanges with the upstream transmission grid and controllable generation units, respectively, actions that the DSO undertakes to relieve local congestion. The third term accounts for the operational costs of grid-connected storage systems, which provide flexibility by charging or discharging during congested periods. The fourth and fifth terms correspond to the costs of procuring flexibility services from industrial parks and IDCs, two key smart prosumers capable of adjusting production or shifting computing loads in response to CM market signals. Finally, the sixth term models the activation costs of the DLC contract, a last-resort measure that the DSO employs when other flexibility options are insufficient. The price of procuring services from smart prosumers ($\lambda^{CM}_{n/d,t}$) is not fixed in advance but is dynamically updated during the adaptive ADMM coordination process until convergence, ensuring that final prices reflect market equilibrium between the DSO and decentralized prosumers. To preserve computational tractability, absolute value expressions in the objective function are represented in linearized form in GAMS.

$$minOF^{DSO} = \sum_t \left[ \begin{array}{c} \varphi^{EM}_t \left| p^{UG}_t - P^{UG,EM}_t \right| + \varphi^{CG}_t \sum_g \left| p^{CG}_{g,t} - P^{CG,EM}_{g,t} \right| \\ + \lambda^{ES} \sum_{es} \left( p^{Ch}_{es,t} + p^{Dis}_{es,t} \right) - \sum_n \left[ \lambda^{CM}_{n,t} \left( \widetilde{P}^{IP}_{n,t} - P^{IP,EM}_{n,t} \right) \right] \\ - \sum_d \left[ \lambda^{CM}_{d,t} \left( \widetilde{P}^{IDC}_{d,t} - P^{IDC,EM}_{d,t} \right) \right] + \lambda^{DLC} \sum_i P^{DLC}_{i,t} \end{array} \right] \Delta t \tag{1}$$

Constraints in (a1) impose operational limits on the active and reactive power outputs of controllable generation units [33]. (a2) calculates the active power generation of PV units, considering installed capacity ($P^{Rate}_{pv}$), conversion efficiency ($\eta^{PV}$), and irradiance rate ($IR_t$). In (a3), the reactive power injected or absorbed by PV units is modeled as a function of the generated active power, adjusted by coefficient $\varphi_{pv}$, which reflects the PV unit's converter capacity to manage reactive power.

$$P^{CG,min}_g \le p^{CG}_{g,t} \le P^{CG,max}_g, Q^{CG,min}_g \le q^{CG}_{g,t} \le Q^{CG,max}_g \tag{a1}$$

$$p^{PV}_{pv,t} = \eta^{PV} \frac{IR_t}{IR^{STC}} P^{Rate}_{pv} \tag{a2}$$

$$-\varphi_{pv} p^{PV}_{pv,t} \le q^{PV}_{pv,t} \le \varphi_{pv} p^{PV}_{pv,t} \tag{a3}$$

Equations (a4)-(a6) model grid-connected energy storage systems. (a4) defines the energy balance, considering both charging and discharging power over time *t*, with efficiencies $\eta^{Ch}$ and $\eta^{Dis}$. (a5) sets the limits on charging and discharging, controlled by binary variables $i^{Ch}_{es,t}$ and $i^{Dis}_{es,t}$, which cannot be simultaneously active. (a6) sets the storage system's energy level to $E^{ES,In}_{es}$ at the start and end of the scheduling period, maintaining it within bounds $E^{ES,min}_{es}$ and $E^{ES,max}_{es}$ during other periods.

$$e^{ES}_{es,t} = e^{ES}_{es,t-1} + \left( p^{Ch}_{es,t} \eta^{Ch} - \frac{p^{Dis}_{es,t}}{\eta^{Dis}} \right) \Delta t \tag{a4}$$

$$0 \le p^{Ch}_{es,t} \le P^{Ch,max}_{es} i^{Ch}_{es,t}, 0 \le p^{Dis}_{es,t} \le P^{Dis,max}_{es} i^{Dis}_{es,t} \tag{a5}$$

$$E^{ES,min}_{es} \le e^{ES}_{es,t} \le E^{ES,max}_{es}, e^{ES}_{es,t=0} = e^{ES}_{es,t=24} = E^{ES,In}_{es} \tag{a6}$$

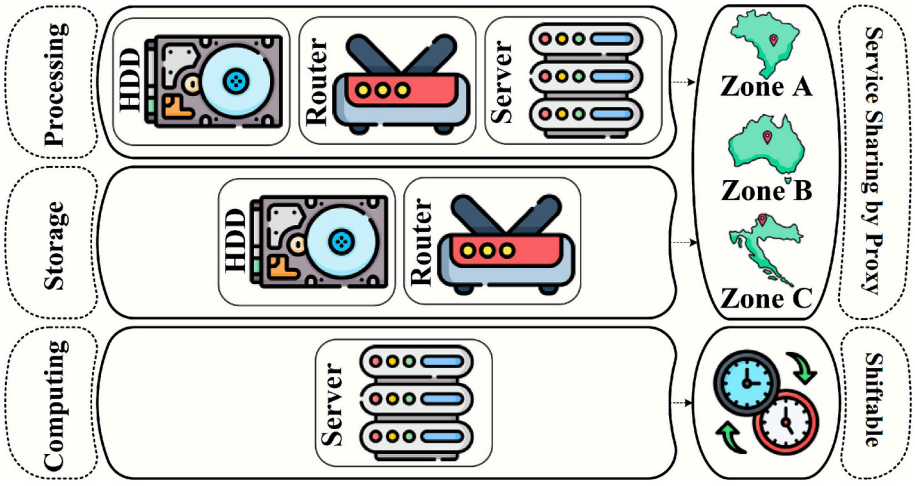


**Fig. 2.** Architecture of Internet data centers.

The linearized AC power flow relations in (a7)-(a14) are essential for identifying potential network congestion [34]. (a7) and (a8) compute active and reactive power flows for each branch, with $G_l$ and $B_l$ representing conductance and susceptance, and $v_{i,t}$ and $\delta_{i,t}$ denoting voltage magnitude and angle. Voltage magnitude and angle constraints are defined in (a9), while (a10) sets bounds on apparent power per branch. The nonlinearity of the quadratic terms, $\left(p_{l,t}^{Line}\right)^2$ and $\left(q_{l,t}^{Line}\right)^2$, is managed through piecewise linearization in GAMS. (a11) calculates hourly power loss per branch, while (a12) and (a13) represent active and reactive power balance equations. Ultimately, (a14) restricts DLC implementation.

$$\frac{p_{l,t}^{Line}}{S^{Base}} = G_l\left(v_{i,t} - v_{j,t}\right) + B_l\left(\delta_{i,t} - \delta_{j,t}\right) \tag{a7}$$

$$\frac{q_{l,t}^{Line}}{S^{Base}} = B_l\left(v_{i,t} - v_{j,t}\right) - G_l\left(\delta_{i,t} - \delta_{j,t}\right) \tag{a8}$$

$$V^{min} \le v_{i,t} \le V^{max}, \delta^{min} \le \delta_{i,t} \le \delta^{max} \tag{a9}$$

$$\left(p_{l,t}^{Line}\right)^2 + \left(q_{l,t}^{Line}\right)^2 \le \left(S_{l,t}^{Line,max}\right)^2 \tag{a10}$$

$$p_{l,t}^{Loss} = \frac{R_l}{\left(S^{Base}\right)^2}\left[\left(p_{l,t}^{Line}\right)^2 + \left(q_{l,t}^{Line}\right)^2\right] \tag{a11}$$

$$p_t^{UG}\big|_{i=1} + \sum_{g\in\Pi_i^g} p_{g,t}^{CG} + \sum_{pv\in\Pi_i^{pv}}\left(p_{pv,t}^{PV} + p_{pv,t}^{Dis,SS} - p_{pv,t}^{Ch,SS}\right) = \sum_{l\in\Pi_i^l}\left(\omega_{i,l} p_{l,t}^{Line}\right) + \sum_{l\in\Pi_i^l}\left(|\omega_{i,l}|\frac{p_{l,t}^{Loss}}{2}S^{Base}\right) + P_{i,t}^{D} - p_{i,t}^{DLC} + \sum_{d\in\Pi_i^d}\tilde{p}_{d,t}^{IDC} + \sum_{n\in\Pi_i^n}\tilde{p}_{n,t}^{IP} \tag{a12}$$

$$q_t^{UG}\big|_{i=1} + \sum_{g\in\Pi_i^g} q_{g,t}^{CG} + \sum_{pv\in\Pi_i^{pv}}\left(q_{pv,t}^{PV}\right) = \sum_{l\in\Pi_i^l}\left(\omega_{i,l} q_{l,t}^{Line}\right) + Q_{i,t}^{D} - \gamma_i p_{i,t}^{DLC} + \sum_{d\in\Pi_i^d}\left(\gamma_d \tilde{p}_{d,t}^{IDC}\right) + \sum_{n\in\Pi_i^n}\left(\gamma_n \tilde{p}_{n,t}^{IP}\right) \tag{a13}$$

$$0 \le P_{i,t}^{DLC} \le v_i P_{i,t}^{D} \tag{a14}$$

### 3.2. Lower level (smart prosumers scheduling)

#### 3.2.1. Internet data centers

Fig. 2 illustrates the architecture of the IDC, which comprises three main service categories, processing, storage, and computing, each organized into multiple clusters [26]. As depicted in the figure, processing and storage services represent non-interruptible tasks that must operate continuously to maintain service quality, whereas computing services are interruptible and can be flexibly rescheduled without affecting user experience. In practice, the IDC participates in the local CM market as a smart prosumer capable of adapting its power consumption in response to signals from the DSO (market organizer). When the DSO identifies congestion, the IDC can shift its computing loads to non-congested time periods or offload part of its non-interruptible services to other data centers located in different geographical areas and time zones via proxy coordination. The IDC's optimization problem, expressed in (2), captures this behavior. The first component of the objective function quantifies the net financial impact of modifying its power exchange in the CM market relative to the pre-settled energy market schedule. The second component represents the costs associated with the service-sharing mechanism, which incorporates the bandwidth usage, latency management, and proxy operation needed to exchange services with other data centers. Together, these terms reflect the IDC's practical decision process: maximizing profitability while flexibly contributing to congestion relief through load shifting and inter-data-center coordination.

$$maxOF_d^{IDC} = \sum_t\left[\lambda_{d,t}^{CM}\left(P_{d,t}^{IDC,EM} - p_{d,t}^{IDC}\right)\right]\Delta t - \sum_s\sum_c\sum_t \lambda_t^{Proxy}\left(\omega_{s,c,d,t}^{Proxy,Out}\right)\Delta t \tag{2}$$

The power consumption ($p_{s,c,d,t}^{IDC}$) of processing, storage, and computing services is constrained in (b1) by a binary variable that defines their active or inactive status ($i_{s,c,d,t}^{IDC}$).

$$p_{s,c,d}^{IDC,min} i_{s,c,d,t}^{IDC} \le p_{s,c,d,t}^{IDC} \le p_{s,c,d}^{IDC,max} i_{s,c,d,t}^{IDC} \tag{b1}$$

Constraints (b2)-(b11) define the operation of non-interruptible services within the IDC, specifically processing and storage tasks. These constraints represent activities that must run continuously to guarantee service quality, forming the backbone of the IDC's baseline workload. Constraint (b2) limits the number of tasks assigned to each Hard Disk Drive (HDD) and router cluster, ensuring that the processing load remains within each cluster's technical capacity. $\chi_{s,c,d,t}^{IDC}$ represents the task count per cluster whereas $\chi_{s,c,d}^{IDC,max}$ represents the maximum number of tasks per cluster. Constraint (b3) manages temporary workload surges by capping them at an upper limit, thereby preventing IDC overloading. Constraint (b4) ensures the continuity of ongoing tasks, so once a process begins, it runs to completion without interruption, reflecting the real-world need to maintain data integrity and user connectivity. Constraint (b5) determines the power consumption of storage

**Table 2**
Service sharing among geo-distributed IDCs.

**Module 1:**
1. Perform ADMM-based CM market settlement in Zone A;
2. **For** IDC $d$ in Zone A, **Do**:
3. Calculate outgoing services from CM market outcomes;
4. Send outgoing services to the proxy; $\rightarrow \omega_{s,c,d,t}^{Proxy,Out}$
5. **End**

**Module 2:**
6. **For** IDC $d$ in Zone B, **Do**:
7. Calculate free capacity for incoming services; $\rightarrow \chi_{s,c,d,t}^{Free} = \chi_{s,c,d}^{IDC,max} - \chi_{s,c,d,t}^{IDC}$
8. Send free capacities to the proxy;
9. **End**

**Module 3:**
10. **For** service $s$, **Do**:
11. **For** task $c$, **Do**:
12. **For** hour $t$, **Do**:
13. Classify services; $\rightarrow \omega_{s,c,t}^{Proxy,High/Med/Low} = \sum_{d \in \Pi^{High/Med/Low}} \omega_{s,c,d,t}^{Proxy,Out}$
14. Classify free capacities; $\rightarrow \chi_{s,c,t}^{Free,High/Med/Low} = \sum_{d \in \Pi^{High/Med/Low}} \chi_{s,c,d,t}^{Free}$
15. **End**
16. **End**
17. **End**

**Module 4:**
18. **For** IDC $d$ in Zone B, **Do**:
19. Allocate services:

$$\xrightarrow{d \in \Pi^{Low}} \omega_{s,c,d,t}^{Proxy,In} = \left( \frac{\chi_{s,c,d,t}^{Free}}{\chi_{s,c,t}^{Free,Low}} \right) \omega_{s,c,t}^{Proxy,Low}$$

$$\xrightarrow{d \in \Pi^{Med}} \omega_{s,c,d,t}^{Proxy,In} = \left( \frac{\chi_{s,c,d,t}^{Free}}{\chi_{s,c,t}^{Free,Med}} \right) \omega_{s,c,t}^{Proxy,Med}$$

$$\xrightarrow{d \in \Pi^{High}} \omega_{s,c,d,t}^{Proxy,In} = \left( \frac{\chi_{s,c,d,t}^{Free}}{\chi_{s,c,t}^{Free,High}} \right) \omega_{s,c,t}^{Proxy,High}$$

20. **End**

**Module 5:**
21. **For** IDC $d$ in Zone B, **Do**:
22. Receive incoming services from the proxy; $\rightarrow \omega_{s,c,d,t}^{Proxy,In}$
23. **End**
24. Perform ADMM-based CM market settlement in Zone B;
25. **For** IDC $d$ in Zone B, **Do**:
26. Calculate outgoing services from CM market outcomes;
27. Send outgoing services to the proxy; $\rightarrow \omega_{s,c,d,t}^{Proxy,Out}$
28. **End**

and router clusters based on their utilization rate, while constraint (b6) calculates the server cluster power consumption ($p_{s,c,d,t}^{IDC}$) as a function of its operational status ($i_{s,c,d,t}^{IDC}$), CPU frequency ($f_{s,c,d,t}^{IDC}$), and utilization rate ($u_{s,c,d,t}$), with power consumption coefficients $A_d$ and $B_d$. These parameters represent the power-performance trade-offs, where higher CPU frequencies and utilization levels increase energy consumption but improve service speed. The non-linear term $\left(f_{s,c,d,t}^{IDC}\right)^3$ is linearized through constraints (b7) and (b8) using a piecewise approximation. The server workload described in (b7) encompasses the aggregated workloads of router and HDD clusters allocated to processing service. $\sigma_{s,c,d,x}^{IDC}$ defines fractional segments of server capacity in the piecewise model, with the binary variable $i_{s,c,d,x,t}^{Freq}$ activating each segment. (b9) defines the utilization rate of each cluster and (b10) constrains it within permissible bounds defined by the maximum utilization rate ($U_{s,c,d}^{max}$). Finally, (b11) enforces Quality of Service (QoS) standards by limiting the server response time ($D_{s,c,d}$).

$$\chi_{s,c,d}^{IDC,min} i_{s,c,d,t}^{IDC} \leq \chi_{s,c,d,t}^{IDC} \leq \chi_{s,c,d}^{IDC,max} i_{s,c,d,t}^{IDC} \tag{b2}$$

$$\sum_s \sum_c \left( \chi_{s,c,d}^{IDC,max} - \chi_{s,c,d,t}^{IDC} \right) \geq CM_d \tag{b3}$$

$$\sum_t \left| i_{s,c,d,t}^{IDC} - i_{s,c,d,t-1}^{IDC} \right| \leq 2 \tag{b4}$$

$$p_{s,c,d,t}^{IDC} = \frac{\chi_{s,c,d,t}^{IDC}}{\chi_{s,c,d}^{IDC,max}} P_{s,c,d}^{IDC,max} \tag{b5}$$

$$p_{s,c,d,t}^{IDC} = B_d i_{s,c,d,t}^{IDC} + A_d \left( f_{s,c,d,t}^{IDC} \right)^3 u_{s,c,d,t} \tag{b6}$$

$$\sum_x \left( \sigma_{s,c,d,x-1}^{IDC} i_{s,c,d,x,t}^{Freq} \right) \leq \sum_{c \in \left\{ \begin{matrix} HDD \\ Router \end{matrix} \right\}} \chi_{s,c,d,t}^{IDC} \leq \sum_x \left( \sigma_{s,c,d,x}^{IDC} i_{s,c,d,x,t}^{Freq} \right) \tag{b7}$$

$$\left( f_{s,c,d,t}^{IDC} \right)^3 = \sum_x \left[ \left( F_{s,c,d,x}^{IDC} \right)^3 i_{s,c,d,x,t}^{Freq} \right] \tag{b8}$$

$$u_{s,c,d,t} = \frac{\chi_{s,c,d,t}^{IDC}}{\chi_{s,c,d}^{IDC,max}} \tag{b9}$$

$$0 \leq u_{s,c,d,t} \leq U_{s,c,d}^{max} \tag{b10}$$

$$i_{s,c,d,t}^{IDC} \leq D_{s,c,d} \left( \chi_{s,c,d}^{IDC,max} - \chi_{s,c,d,t}^{IDC} \right) \tag{b11}$$

Constraints (b12) and (b13) model computing services as interruptible activities that can be rescheduled over time. (b12) computes the power consumption of the server allocated for computing, considering its full-load consumption ($P_{s,c,d}^{IDC}$) and a modulation factor $z_{s,c,d,t}^{IDC}$ (ranging from 0 to 1) to adjust consumption dynamically over time. The sum of $z_{s,c,d,t}^{IDC}$ over the scheduling horizon must be equal to $\varpi_d^{IDC}$, representing the

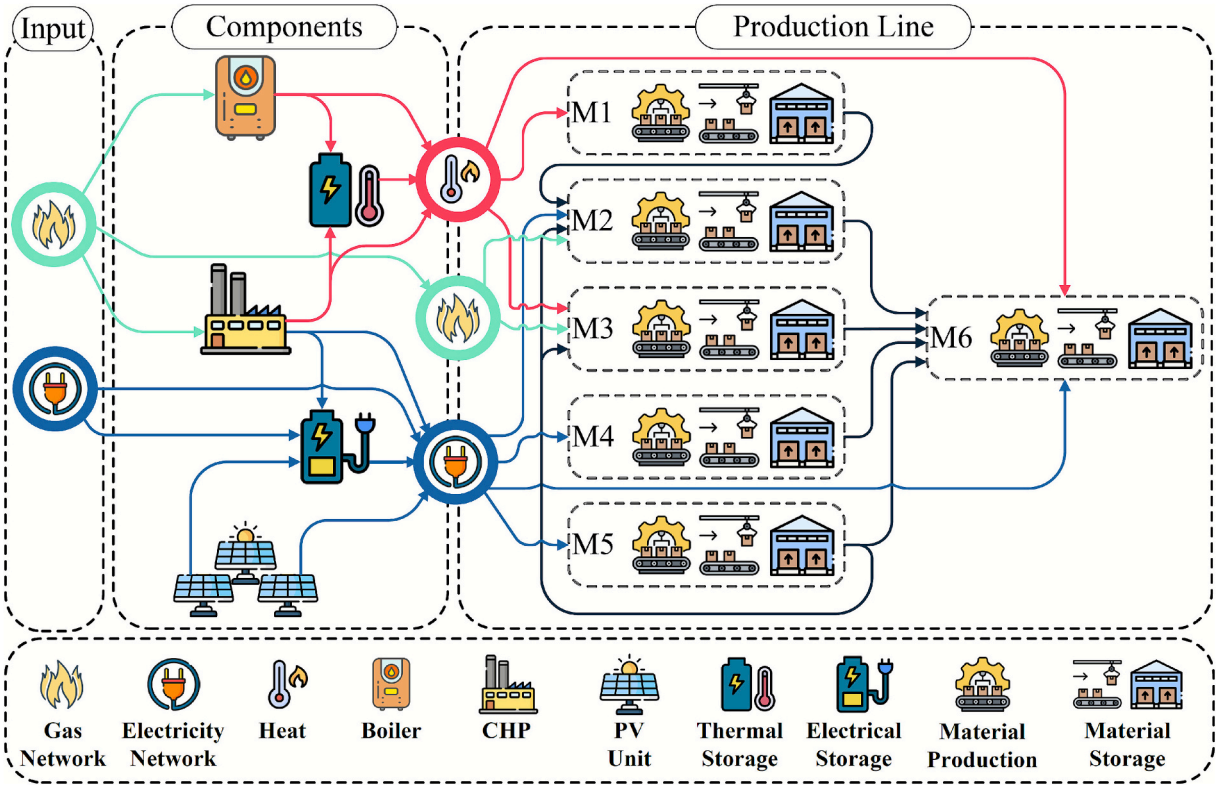


**Fig. 3.** Architecture of the industrial parks.

predefined computing service requirements. (b13) ensures that the computing server is on whenever $z^{IDC}_{s,c,d,t}$ is nonzero.

$$p^{IDC}_{s,c,d,t} = P^{IDC}_{s,c,d} z^{IDC}_{s,c,d,t}, \sum_t \sum_s \sum_c z^{IDC}_{s,c,d,t} = \varpi^{IDC}_d \tag{b12}$$

$$0 \le z^{IDC}_{s,c,d,t} \le i^{IDC}_{s,c,d,t} \tag{b13}$$

Constraints (b14)-(b18) model the air-conditioning system to regulate IDC cooling. Constraint (b14) defines the air-conditioning system's allowable power consumption range. Equation (b15) relates the air-conditioning output temperature ($\theta^{Output}_{d,t}$) to the indoor temperature ($\theta^{Indoor}_{d,t}$), considering operational efficiency ($\eta^{AC}_d$) and inertia ($\varepsilon$). Equation (b16) defines the indoor temperature as a function of the cooling output and the heat released by IDC activities ($\frac{\sum_s \sum_c p^{IDC}_{s,c,d,t}}{\rho C^p \psi_d}$). $\psi_d$ denotes the airflow rate, whereas $\rho$ and $C^p$ represent air density and specific heat capacity, respectively. Constraint (b17) deactivates the air-conditioning system at the minimum indoor temperature ($\theta^{min}_d$), while (b18) sets it to rated capacity at the peak temperature ($\theta^{max}_d$).

$$P^{AC,min}_d \le p^{AC}_{d,t} \le P^{AC,max}_d \tag{b14}$$

$$\theta^{Output}_{d,t} = \varepsilon \theta^{Output}_{d,t-1} + (1-\varepsilon)\left(\theta^{Indoor}_{d,t} - \eta^{AC}_d p^{AC}_{d,t}\right) \tag{b15}$$

$$\theta^{Indoor}_{d,t} = \theta^{Output}_{d,t} + \frac{\sum_s \sum_c p^{IDC}_{s,c,d,t}}{\rho C^p \psi_d} \tag{b16}$$

$$\theta^{Output}_{d,t} - \theta^{min}_d \ge M\left(i^{AC}_{d,t} - 1\right) \tag{b17}$$

$$\left(o^{AC}_{d,t} - 1\right)M \le \theta^{max}_d - \theta^{Output}_{d,t} \le o^{AC}_{d,t} M, p^{AC}_{d,t} \ge P^{AC,max}_d \left(1 - o^{AC}_{d,t}\right) \tag{b18}$$

Equation (b19) models the workload balance for non-interruptible services, where $\omega^{IDC}_{s,c,d,t}$ represents the workload before service sharing, and $\omega^{Proxy,Out}_{s,c,d,t}$ and $\omega^{Proxy,In}_{s,c,d,t}$ denote services sent to and received from the proxy, respectively. It is assumed that each IDC can transfer up to 25 % of its non-interruptible services to a proxy and receive services based on available capacity. The proxy then distributes these services among geographically distributed IDCs located in different time zones. Equation (b20) defines the IDC's power balance, considering grid exchanges ($p^{IDC}_{d,t}$), internal consumption ($p^{IDC}_{s,c,d,t}$), and PV system.

$$\chi^{IDC}_{s,c,d,t} = \omega^{IDC}_{s,c,d,t} + \omega^{Proxy,In}_{s,c,d,t} - \omega^{Proxy,Out}_{s,c,d,t} \tag{b19}$$

$$p^{IDC}_{d,t} = \sum_s \sum_c p^{IDC}_{s,c,d,t} - p^{PV}_{d,t} \tag{b20}$$

Table 2 outlines the service-sharing process among IDCs across three time zones: A (Brazil), B (Spain), and C (Australia). Each zone settles its market independently, with Zone A operating 5 h behind Zone B and Zone C 8 h ahead. IDCs are categorized into low, medium, and high priority, with proxy services dispatched exclusively within the same priority level. The process begins in Module 1, where markets in Zone A are assumed to be settled, and IDCs submit their outgoing services to the proxy. Module 2 involves pre-scheduling by IDCs in Zone B to determine their available free capacities, which are then communicated to the proxy. Here, $\chi^{IDC,max}_{s,c,d}$ represents the maximum capacity of clusters in storage and processing services, while $\chi^{IDC}_{s,c,d,t}$ denotes their occupied capacity. In Module 3, the proxy classifies these free capacities and outgoing services based on IDC type, service type, cluster, and execution time. Subsequently, in Module 4, the proxy allocates services from Zone A to the available free capacities in Zone B. Finally, in Module 5, the IDCs in Zone B compute and submit their outgoing services to the proxy after settling the CM market. Coordination between Zones B and C follows the same sequence as Modules 2 to 5, substituting Zone A with B and Zone B with C.

### 3.2.1. Industrial parks

Fig. 3 illustrates the structure of the industrial parks considered in

this study. Each park is connected to both the electricity and natural gas networks at their entry points and integrates multiple DERs, including PV units, CHP systems, boilers, and electrical and thermal energy storage systems. These components jointly supply the electricity and heat required to produce a sequence of intermediate materials (1–6), where each material represents a specific stage in the production process and is temporarily stored before being used in the next stage. The last material, Material 6, corresponds to the final product sold in the market.

In the local CM market, the industrial park operates as a smart prosumer capable of adjusting its internal energy use and production schedule in response to coordination signals received from the DSO (market organizer). This flexibility enables the industrial park to modulate its electricity consumption over the scheduling horizon, either increasing or decreasing it as required, with reductions specifically occurring during congested periods to deliver downward services to the grid, while ensuring that overall daily production objectives are fully met. The objective function in Eq. (3) mathematically represents this behavior. Its first term quantifies the profit (or cost) derived from modifying power exchanges between the energy and CM markets, reflecting how the park's adjusted operation contributes to congestion relief. The second term models the cost of changes in gas consumption associated with these operational adjustments. Note that any variation in gas purchases relative to the pre-settled energy market schedule leads to a proportional cost correction.

$$maxOF_n^{IP} = \sum\nolimits_t \left[\lambda_{n,t}^{CM}\left(P_{n,t}^{IP,EM} - p_{n,t}^{IP}\right)\right]\Delta t - \sum\nolimits_t \left[\lambda_t^{Gas}\left(g_{n,t}^{IP} - G_{n,t}^{IP,EM}\right)\right]\Delta t \quad (3)$$

The operational limits of the CHP system define a trapezoidal region with vertices *A*, *B*, *C*, and *D*, representing the relationship between heat and electricity generation. Constraint (c1) ensures the operating point remains under the boundary represented by line *AB*. Additional boundaries are introduced by constraints (c2) and (c3), restricting operation within the regions demarcated by lines *BC* and *CD*, respectively. Moreover, constraints (c4) provide further restrictions on both heat and electricity generation. Finally, gas consumption for the CHP unit is defined through (c5).

$$p_{n,t}^{CHP} - P_n^A - \frac{P_n^A - P_n^B}{H_n^A - H_n^B}\left(h_{n,t}^{CHP} - H_n^A\right) \le 0 \quad (c1)$$

$$p_{n,t}^{CHP} - P_n^B - \frac{P_n^B - P_n^C}{H_n^B - H_n^C}\left(h_{n,t}^{CHP} - H_n^B\right) \ge -\left(1 - i_{n,t}^{CHP}\right)M \quad (c2)$$

$$p_{n,t}^{CHP} - P_n^C - \frac{P_n^C - P_n^D}{H_n^C - H_n^D}\left(h_{n,t}^{CHP} - H_n^C\right) \ge -\left(1 - i_{n,t}^{CHP}\right)M \quad (c3)$$

$$0 \le h_{n,t}^{CHP} \le H_n^B i_{n,t}^{CHP}, P_n^C i_{n,t}^{CHP} \le p_{n,t}^{CHP} \le P_n^A i_{n,t}^{CHP} \quad (c4)$$

$$g_{n,t}^{CHP} = \frac{p_{n,t}^{CHP}}{\eta_n^{CHP,ge}} + \frac{h_{n,t}^{CHP}}{\eta_n^{CHP,gh}} \quad (c5)$$

Equation (c6) models the heat generation of the boiler, where the thermal output ($h_{n,t}^B$) depends on gas consumption ($g_{n,t}^B$) and efficiency factor ($\eta_n^{B,gh}$). (c7) imposes an upper limit on heat generation, ensuring it does not exceed the boiler's maximum capacity ($H_n^{B,max}$). Note that electrical and thermal storage systems in industrial parks are formulated similarly to grid-connected electrical storage systems.

Equations (c8)-(c21) define the hourly power, heat, and gas flows within the industrial park. (c8) governs the power exchange direction between the industrial park and the grid, based on variables $p_{n,t}^{IP,Buy}$ and $p_{n,t}^{IP,Sell}$, which are subject to non-simultaneity constraints. The values of $p_{n,t}^{IP,Buy}$ and $p_{n,t}^{IP,Sell}$ are determined by (c9) and (c10), respectively. Equation (c11) manages the power output balance of the PV system. Equations (c12) and (c13) handle input and output power balances for the electrical storage system, while (c14) and (c15) manage thermal storage balances. Equations (c16) and (c17) model the power and heat balance of the CHP system, and (c18) addresses the heat balance for boiler output. Equation (c19) calculates gas flow into the industrial park, accounting for consumption by the CHP, boiler, and materials production processes. Equation (c20) models electricity consumption for fixed loads and material production, and (c21) captures the corresponding heat consumption for these processes.

$$h_{n,t}^B = \eta_n^{B,gh} g_{n,t}^B \quad (c6)$$

$$h_{n,t}^B \le H_n^{B,max} \quad (c7)$$

$$p_{n,t}^{IP} = p_{n,t}^{IP,Buy} - p_{n,t}^{IP,Sell} \quad (c8)$$

$$p_{n,t}^{IP,Buy} = p_{n,t}^{Grid\to L} + p_{n,t}^{Grid\to ES} \quad (c9)$$

$$p_{n,t}^{IP,Sell} = p_{n,t}^{PV\to Grid} + p_{n,t}^{CHP\to Grid} + p_{n,t}^{ES\to Grid} \quad (c10)$$

$$P_{n,t}^{PV} = p_{n,t}^{PV\to Grid} + p_{n,t}^{PV\to ES} + p_{n,t}^{PV\to L} \quad (c11)$$

$$p_{n,t}^{ES,Ch} = p_{n,t}^{Grid\to ES} + p_{n,t}^{PV\to ES} + p_{n,t}^{CHP\to ES} \quad (c12)$$

$$p_{n,t}^{ES,Dis} = p_{n,t}^{ES\to Grid} + p_{n,t}^{ES\to L} \quad (c13)$$

$$h_{n,t}^{TS,Ch} = h_{n,t}^{CHP\to TS} + h_{n,t}^{B\to TS} \quad (c14)$$

$$h_{ts,t}^{TS,Dis} = h_{n,t}^{TS\to L} \quad (c15)$$

$$p_{n,t}^{CHP} = p_{n,t}^{CHP\to Grid} + p_{n,t}^{CHP\to ES} + p_{n,t}^{CHP\to L} \quad (c16)$$

$$h_{ip,t}^{CHP} = h_{n,t}^{CHP\to TS} + h_{n,t}^{CHP\to L} \quad (c17)$$

$$h_{ip,t}^B = h_{n,t}^{B\to TS} + h_{n,t}^{B\to L} \quad (c18)$$

$$g_{n,t}^{IP} = g_{n,t}^{(T1-T6)} + g_{n,t}^{CHP} + g_{n,t}^B \quad (c19)$$

$$p_{n,t}^{ES\to L} + p_{n,t}^{CHP\to L} + p_{n,t}^{Grid\to L} + p_{n,t}^{PV\to L} = p_{n,t}^{(T1-T6)} + P_{n,t}^{Fixed} \quad (c20)$$

$$h_{n,t}^{TS\to L} + h_{n,t}^{CHP\to L} + h_{n,t}^{GB\to L} = h_{n,t}^{(T1-T6)} + H_{n,t}^{Fixed} \quad (c21)$$

The materials production process within the industrial park is formulated in (c22)-(c32) and represents the coordinated operation of sequential production stages, as illustrated in Fig. 3. Equations (c22)-(c27) describe the conversion processes through which intermediate materials (1–6) are produced, where parameter $W^{P/G/H/M,T(.)}$ translates the energy consumed by industrial equipment into material output. This formulation captures the physical relationship between energy use and production rate in each stage of the manufacturing chain. Equation (c28) imposes hourly limits on production increases or decreases for the final product (Material 6), reflecting the technical constraints and ramping capabilities of industrial processes. Equation (c29) ensures that the total production of the final product over the scheduling horizon equals a predefined target, meaning that temporary adjustments in production, such as reductions during congested periods to provide downward services, are later compensated to maintain the total daily output. Equation (c30) models the storage dynamics of materials 1–6, considering the balance between previously stored volumes, newly produced materials, and those transferred between stages. Equations (c31) and (c32) define the storage capacity limits and initial inventory levels, ensuring that all production and storage activities remain within feasible operational boundaries.

$$m_{n,t}^{Prod,T1} = W^{H,T1} p_{n,t}^{T1} \quad (c22)$$

$$m_{n,t}^{Prod,T2} = W^{P,T2} p_{n,t}^{T2} + W^{G,T2} g_{n,t}^{T2} + W^{M1,T2} m_{n,t}^{M1,T2} + W^{M5,T2} m_{n,t}^{M5,T2} \quad (c23)$$

**Table 3**
Pseudocode of the proposed adaptive ADMM for market coordination.

1. **Set** starting point for coupling variables;→$p_{d,t}^{IDC}$ ,$p_{n,t}^{IP}$, $\lambda_{d,t,it}^{CM}$, $\lambda_{n,t,it}^{CM}$
2. **Add** penalty terms to agents' objectives; →$\left\|\widetilde{p}_{d,t}^{IDC}-p_{d,t}^{IDC}\right\|_2^2$, $\left\|\widetilde{p}_{n,t}^{IP}-p_{n,t}^{IP}\right\|_2^2$
3. $it = 1$; $Stop = 0$
4. **While** ($Stop \neq 1$), **Do**:
5. $it \leftarrow it+1$
6. **Minimize** $OF^{DSO}$ subject to constraints (a1)-(a14);
7. **For** IDC $d$, **Do**:
8. **Update** IDC's workload with services from proxy; →$\omega_{s,c,d,t}^{Proxy,In}$
9. **Maximize** $OF_d^{IDC}$ subject to (b1) to (b20);
10. **End**
11. **For** industrial park $n$, **Do**:
12. **Maximize** $OF_n^{IP}$ subject to constraints (c1) to (c32);
13. **End**
14. **Update** service prices at connection points;→$\lambda_{d/n,t}^{CM,it+1} = \lambda_{d/n,t}^{CM,it} + \rho^{IDC/IP}\left(p_{d/n,t}^{IDC/IP}-\widetilde{p}_{d/n,t}^{IDC/IP}\right)$
15. **Calculate** primal residuals (Eq. d3); →$r^{P,IDC/IP} = \left\|\widetilde{p}_{d/n,t}^{IDC/IP}-p_{d/n,t}^{IDC/IP}\right\|_2^2$
16. **Calculate** dual residuals (Eq. d4); →$r^{D,\frac{IDC}{IP}} = \left\|\lambda_{\frac{d}{n},t}^{CM,it}-\lambda_{\frac{d}{n},t}^{CM,it-1}\right\|_2^2$
17. **Switch** ($\gamma = \frac{r^{P,IDC/IP}}{r^{D,IDC/IP}}$)
18. **Case** $\gamma \geq \gamma^{max}$; →$\rho^{\frac{IDC}{IP}} = \alpha\rho^{\frac{IDC}{IP}}$
19. **Case** $\gamma \leq \gamma^{min}$; →$\rho^{\frac{IDC}{IP}} = \frac{\rho^{\frac{IDC}{IP}}}{\beta}$
20. **Default**; → do not update;
21. **End**
22. **If** ($r^{P,IDC}+r^{P,IP} \leq \varepsilon$), **Then**:
23. $Stop = 1$;
24. **End**
25. **End**
26. **Send** outgoing services to the proxy;→$\omega_{s,c,d,t}^{Proxy,Out}$

$$m_{n,t}^{Prod,T3} = W^{H,T3}p_{n,t}^{T3} + W^{G,T3}g_{n,t}^{T3} + W^{M5,T3}m_{n,t}^{M5,T3} \tag{c24}$$

$$m_{n,t}^{Prod,T4} = W^{P,T4}p_{n,t}^{T4} \tag{c25}$$

$$m_{n,t}^{Prod,T5} = W^{P,T5}p_{n,t}^{T5} \tag{c26}$$

$$m_{n,t}^{Prod,T6} = W^{P,T6}p_{n,t}^{T6} + W^{H,T6}h_{n,t}^{T6} + W^{M2,T6}m_{n,t}^{M2,T6} + W^{M3,T6}m_{n,t}^{M3,T6} + W^{M4,T6}m_{n,t}^{M4,T6} + W^{M5,T6}m_{n,t}^{M5,T6} \tag{c27}$$

$$M_{n,t}^{min,T6} \leq m_{n,t}^{Prod,T6} \leq M_{n,t}^{max,T6} \tag{c28}$$

$$\sum\nolimits_t m_{n,t}^{Prod,T6} = \sum\nolimits_t M_{n,t}^{Prod,Desire} \tag{c29}$$

$$e_{n,t}^{(T1-T6)} = e_{n,t-1}^{(T1-T6)} + m_{n,t}^{Prod,(T1-T6)} - m_{n,t}^{Used,(T1-T6)} \tag{c30}$$

$$E_n^{(T1-T6),min} \leq e_{n,t=0}^{(T1-T6)} \leq E_n^{(T1-T6),max} \tag{c31}$$

$$e_{n,t=0}^{(T1-T6)} = E_n^{(T1-T6),In} \tag{c32}$$

### 3.2.2. Distributed coordination of market agents

The proposed adaptive ADMM enables decentralized coordination between upper and lower levels, structured through (d1)-(d5). This method introduces penalty terms into the objective functions of market agents, including the DSO, IDCs, and industrial parks. Specifically, (d1) specifies the penalty terms for IDCs and industrial parks, which are included in their respective objective functions and jointly integrated into the DSO's objective function. These terms are dynamically updated at each iteration based on variations in the coupling variables and penalty parameters ($\rho^{IDC}$ and $\rho^{IP}$). The variables without a tilde ($p_{d/n,t}^{IDC/IP}$) denote the local decisions of the prosumers, while those with a tilde ($\widetilde{p}_{d/n,t}^{IDC/IP}$) correspond to the coupling variables optimized by the DSO. According to (d2), exchange prices between the DSO and smart prosumers are iteratively adjusted based on the discrepancies in defined coupling variables. The primal residual is derived from coupling variable differences as outlined in (d3), while (d4) determines the dual residual based on price variations across iterations. Equation (d5) updates the penalty parameter automatically to keep the primal and dual residuals at a similar scale. This helps the algorithm progress steadily in price updates, leading to faster and more stable convergence under different system conditions. Specifically, the penalty parameter is adjusted by applying a multiplicative factor $\alpha$ when the primal residual ($r^{P,IDC/IP}$) significantly exceeds the dual residual ($r^{D,IDC/IP}$), and divided by $\beta$ when the opposite occurs. An extensive series of simulation runs indicated that setting $\alpha$ and $\beta$ to 1.1 and 1.2, respectively, results in the most robust and fastest convergence behavior of the proposed algorithm. Table 3 presents a pseudocode of the proposed adaptive ADMM for coordinating market agents. The algorithm stops when the sum of the primal residuals falls below the specified threshold ($\varepsilon = 2\times10^{-2}$).

$$\frac{\rho^{IDC}}{2}\left\|\widetilde{p}_{d,t}^{IDC}-p_{d,t}^{IDC}\right\|_2^2, \frac{\rho^{IP}}{2}\left\|\widetilde{p}_{n,t}^{IP}-p_{n,t}^{IP}\right\|_2^2 \tag{d1}$$

$$\lambda_{d/n,t}^{CM,it+1} = \lambda_{d/n,t}^{CM,it} + \rho^{IDC/IP}\left(p_{d/n,t}^{IDC/IP}-\widetilde{p}_{d/n,t}^{IDC/IP}\right) \tag{d2}$$

$$r^{P,IDC/IP} = \left\|\widetilde{p}_{d/n,t}^{IDC/IP}-p_{d/n,t}^{IDC/IP}\right\|_2^2 \tag{d3}$$

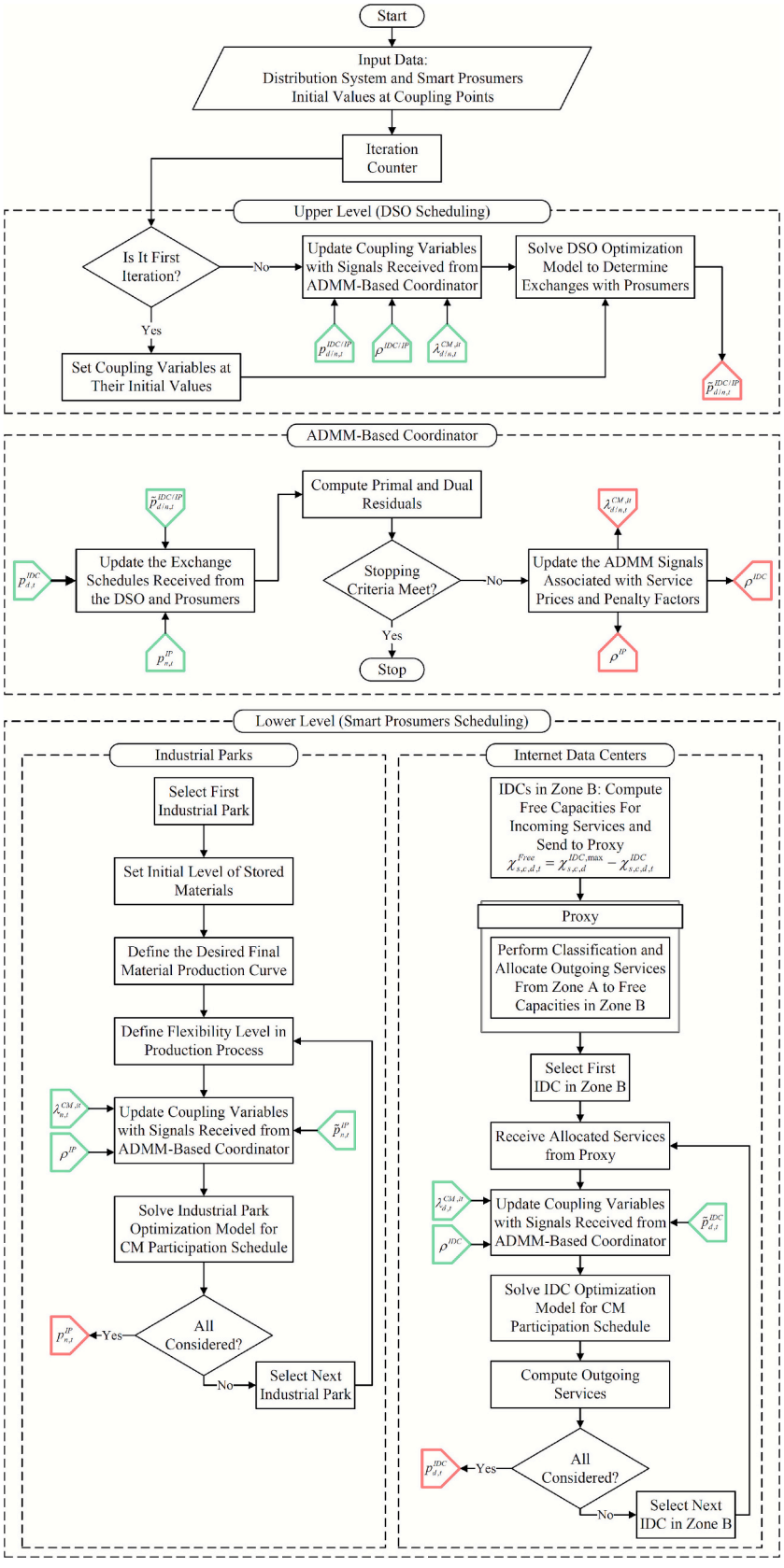


**Fig. 4.** Implementation workflow of the proposed distributed optimization framework.

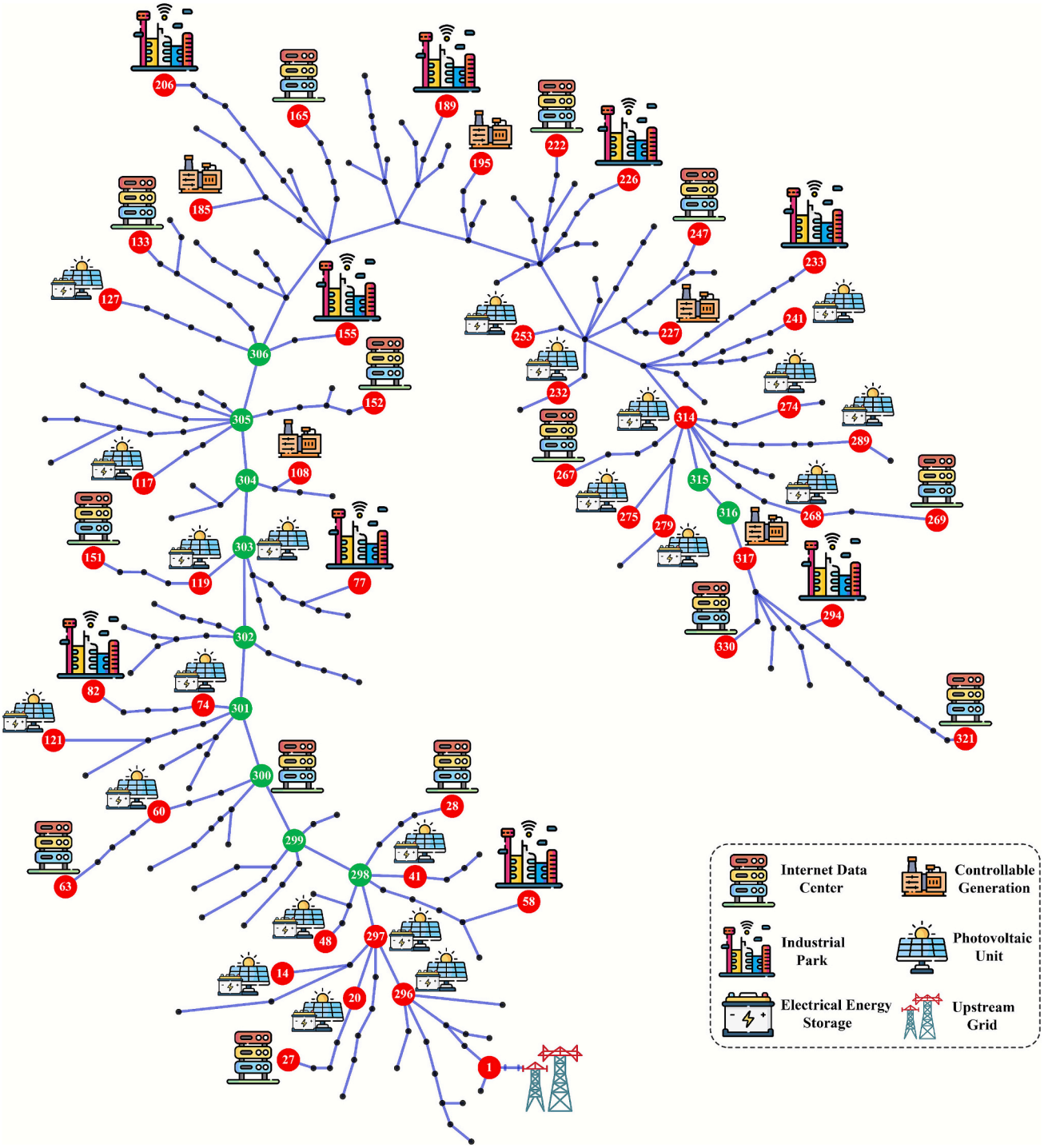


**Fig. 5.** 334-Bus case study in Alcalá de Henares, Spain.

$$r^{D,IDC/IP} = \left\| \lambda_{d/n,t}^{CM,it} - \lambda_{d/n,t}^{CM,it-1} \right\|_2^2 \tag{d4}$$

$$\rho^{IDC/IP} = \begin{cases} \alpha\rho^{IDC/IP}, & r^{P,IDC/IP} >> r^{D,IDC/IP} \\ \rho^{IDC/IP}/\beta, & r^{D,IDC/IP} >> r^{P,IDC/IP} \\ \rho^{IDC/IP}, & \text{Otherwise} \end{cases} \tag{d5}$$

## 4. Proposed model implementation

Fig. 4 depicts the implementation workflow of the proposed bi-level distributed optimization mechanism, which coordinates the DSO and smart prosumers through an adaptive ADMM. The process operates iteratively across three layers: the upper-level DSO scheduling, the ADMM-based coordination layer, and the lower-level smart prosumer scheduling. At the upper level, the DSO receives updated coordination signals from the ADMM layer, which include exchanged power and dual price variables, and solves its local congestion management problem to determine revised power exchanges with prosumers. In the first iteration, the DSO initializes the coupling variables with predefined values to initiate the coordination process. In subsequent iterations, these variables are updated based on the exchanged information between the DSO and the smart prosumers, continuing until convergence is achieved. The

**Table 4**
Key parameters used in the simulation.

| Parameter | Value (unit) | Parameter | Value (unit) | Parameter | Value (unit) |
|---|---|---|---|---|---|
| $\alpha$ | 1.1 | $\eta^{Ch}$ | 98 (%) | $V^{min}$ | 0.9 (p.u) |
| $\beta$ | 1.2 | $\eta^{Dis}$ | 98 (%) | $V^{max}$ | 1.1 (p.u) |
| $C^p$ | 1.005 (kJ/kg.°C) | $IR^{STC}$ | 1000 (W/m$^2$) | $S^{Base}$ | $10^5$ |
| $\Delta t$ | 1 (h) | $\lambda^{DLC}$ | 10 ($/kWh) | $\gamma_i/\gamma_d/\gamma_n$ | 0.46 (kVAR/kW) |
| $\delta^{min}$ | $-\pi$(rad) | $\rho$ | 1.19 (kg/m$^3$) | $\eta^{PV}$ | 98 (%) |
| $\delta^{max}$ | $\pi$(rad) | $M$ | $10^5$ | $\lambda^{ES}$ | 0.05 ($/kWh) |

coordination layer implements the adaptive ADMM algorithm, which manages the interaction between the DSO and prosumers. At each iteration, the coordinator evaluates the primal and dual residuals, updates the penalty parameters dynamically, and redistributes the adjusted variables to all agents. This adaptive update mechanism accelerates convergence and maintains numerical stability. At the lower level, smart prosumers, industrial parks, and IDCs optimize their internal operations in response to the received ADMM signals. Industrial parks coordinate their distributed energy resources and production schedules to provide congestion management services, while IDCs perform load-shifting and service-sharing operations through a proxy system that links geographically distributed centers. The updated power exchanges from all prosumers are then sent back to the coordinator, completing one iteration of the ADMM loop. The signal indicators in the figure distinguish between input (red) and output (green) exchanges among entities, emphasizing the iterative and privacy-preserving communication that leads to global market equilibrium. This workflow ensures optimal coordination with minimal information sharing, achieving convergence efficiency and scalability in large distribution systems.

## 5. Simulation results

The proposed mechanism is implemented on a real case study in Alcalá de Henares, Spain. This case study, illustrated in Fig. 5, involves a 334-bus distribution system connected to 9 industrial parks and 14 IDCs. The network load is supplied through the upstream grid, five fossil-fueled controllable generators and twenty-two PV units. Each PV unit is paired with a dedicated storage system. Subscribers at 11 buses, highlighted in green, are under DLC contracts, allowing the DSO to disconnect their load during emergencies or congestion for a predetermined price. The key parameters employed in the simulation are reported in Table 4. The information on the industrial parks, IDCs, network components, and network nodes is provided in Table 5. Furthermore, comprehensive information regarding the network nodes, network components, and smart prosumers is available online in [35].

The proposed mechanism is evaluated under four scenarios summarized in Table 6. Scenario 1 represents the base case, where the DSO

**Table 5**
Information on industrial parks, IDCs, network components, and network nodes.

**Industrial Parks**

| Type | Node Number | Capacity of Power & Thermal Generation Units (kW) | | | Capacity of Storage Systems (kWh) | | Final Product (units/day) | Daily Fixed Energy Demand (kWh) | |
|---|---|---|---|---|---|---|---|---|---|
| | | CHP | Boiler | PV | Electrical | Thermal | | Electrical | Thermal |
| 1 | 58, 155, 226 | 600 | 1000 | 700 | 100 | 700 | 28,800 | 13,102.34 | 7981.06 |
| 2 | 82, 206, 233 | 800 | 900 | 600 | 200 | 500 | 33,600 | 9353.82 | 8296.86 |
| 3 | 77, 189, 294 | 600 | 1000 | 1000 | 200 | 600 | 36,000 | 11,192.24 | 6242.13 |

**Internet Data Centers**

| Type | Node Number | Processing (tasks/day) | | Storage (tasks/day) | | Computing | | |
|---|---|---|---|---|---|---|---|---|
| | | HDD | Router | HDD | Router | Workload (h) | Power Usage (kWh) | PV Capacity (kW) |
| 1 | 300, 63, 133 247, 269 | 1200 | 1100 | 1100 | 970 | 11 | 1925 | 200 |
| 2 | 27, 151, 165 267, 321 | 1300 | 1000 | 1000 | 900 | 12 | 2100 | 250 |
| 3 | 28, 152, 222 330 | 1300 | 600 | 1000 | 1200 | 14 | 2450 | 200 |

**Network Components**

| PV Units | | | | Electrical Storage Systems | | | |
|---|---|---|---|---|---|---|---|
| Node Number | Capacity (kW) | Node Number | Capacity (kW) | Node Number | Capacity (kWh) | Node Number | Capacity (kWh) |
| 48 | 400 | 303 | 350 | 48 | 400 | 303 | 375 |
| 60 | 450 | 41 | 450 | 60 | 425 | 41 | 425 |
| 275 | 350 | 117 | 350 | 275 | 375 | 117 | 375 |
| 289 | 400 | 274 | 300 | 289 | 400 | 274 | 350 |
| 119 | 450 | 279 | 500 | 119 | 425 | 279 | 450 |
| 121 | 500 | 296 | 450 | 121 | 450 | 296 | 425 |
| 14 | 400 | 232 | 450 | 14 | 400 | 232 | 425 |
| 20 | 350 | 74 | 400 | 20 | 375 | 74 | 400 |
| 253 | 450 | 268 | 350 | 253 | 425 | 268 | 375 |
| 297 | 350 | 127 | 500 | 297 | 375 | 127 | 450 |
| 241 | 300 | 314 | 450 | 241 | 350 | 314 | 425 |

| Controllable Generators | |
|---|---|
| Node Number | Capacity (kW) |
| 317, 227, 195, 185, 108 | 1500, 1200, 1275, 1350, 1500 |

**Network Nodes**

| Nodes with Inflexible Demand (PQ) | Nodes Under DLC Contract (PQ) |
|---|---|
| 1–26, 29–57, 59–62, 64–76, 78–81, 83–132, 134–150, 153, 154 156–164, 166–188, 190–205, 207–221, 223–225, 227–232 234–246, 248–266, 268, 270–293, 295–297, 307–314 317–320, 322–329, 331–334 | 298–306, 315, 316 |

**Table 6**
Definition of the studied scenarios.

| Scenarios | Available Resources for Congestion Management | | | |
|---|---|---|---|---|
| | Controllable Generators & DLC Contracts | Grid-Connected Storage Systems | Industrial Parks | IDCs |
| 1 | ✓ | × | × | × |
| 2 | ✓ | ✓ | × | × |
| 3 | ✓ | ✓ | ✓ | × |
| 4 | ✓ | ✓ | ✓ | ✓ |

relies only on controllable generators and DLC contracts to provide congestion management services. Scenarios 2–4 progressively incorporate additional flexibility resources that can deliver congestion management services: grid-connected storage systems in Scenario 2, industrial parks in Scenario 3, and IDCs in Scenario 4. This stepwise design enables the assessment of how the inclusion of each resource type enhances the DSO's capability to manage network congestion under comparable operating conditions.

Table 7 presents the numerical outputs from simulations of Scenarios 1 to 4. In Scenario 1, the DSO's options for resolving congestion include modifying exchanges with the upstream grid, adjusting the production of local controllable generators, and deploying DLC contracts. Scenario 2 adds storage systems to these options. It is worth noting that DLC is the costliest strategy available to the DSO and is used as a last resort for congestion alleviation. The numerical results indicate that the DSO's congestion relief costs in Scenario 2, with storage systems available, decreased by 8.64 % compared to Scenario 1. This reduction is attributed to a 21.27 % decrease in the need for DLC implementation.

Fig. 6a and b illustrate the services employed to alleviate congestion during the morning and evening periods for Scenarios 1 and 2, along with the corresponding power exchange curves with the upstream grid in both the energy and CM markets. In Scenario 1, despite the increased output of controllable generators during congestion, the DSO was required to reduce upstream purchases and curtail the load of certain DLC subscribers. In Scenario 2, although a similar strategy was adopted, access to storage systems substantially reduced DLC-related load interruptions. It is observed that the storage systems charge during non-congested periods and discharge during congested periods, thereby mitigating the reliance on DLC-based interventions.

In the third scenario, industrial parks act as smart prosumers providing grid services in the CM market. Table 7 indicates that by offering downward services in the CM market, industrial parks in Scenario 3 gained a profit of $26,998.59. Additionally, the provision of these services reduced the DSO's congestion alleviation costs by 10.8 % compared to Scenario 2, primarily due to the lower cost of procuring services from industrial parks compared to the cost of implementing DLC contracts. Fig. 7 illustrates the congestion relief measures in Scenario 3, where a significant portion of DLC interventions was replaced by downward services from industrial parks. However, reductions in upstream purchases during both congestion periods were unavoidable due to capacity constraints on lines. Fig. 8a and b present the electrical and

**Table 7**
Numerical outcomes of Scenarios 1–4.

| Sc. | Controllable Generations ($) | DLC ($) | Storage Systems ($) | Industrial Parks ($) | IDCs ($) | Sum ($) |
|---|---|---|---|---|---|---|
| 1 | 11,466.04 | 64,003.70 | 0 | 0 | 0 | 97,303.08 |
| 2 | 11,466.01 | 50,389.63 | 764.16 | 0 | 0 | 88,891.08 |
| 3 | 7632.12 | 6859.61 | 596.63 | 26,998.59 | 0 | 79,282.16 |
| 4 | 3016.47 | 0 | 382.08 | 9774.86 | 7117.76 | 57,536.21 |

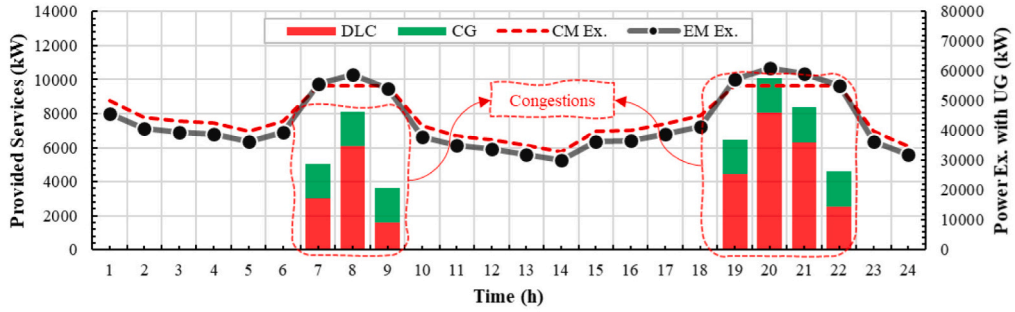


(a) Scenario 1

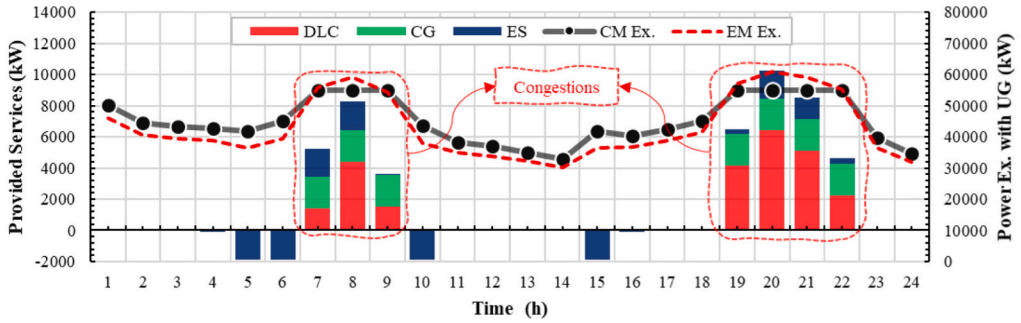


(b) Scenario 2

**Fig. 6.** Grid services used for congestion relief in Scenarios 1 & 2.

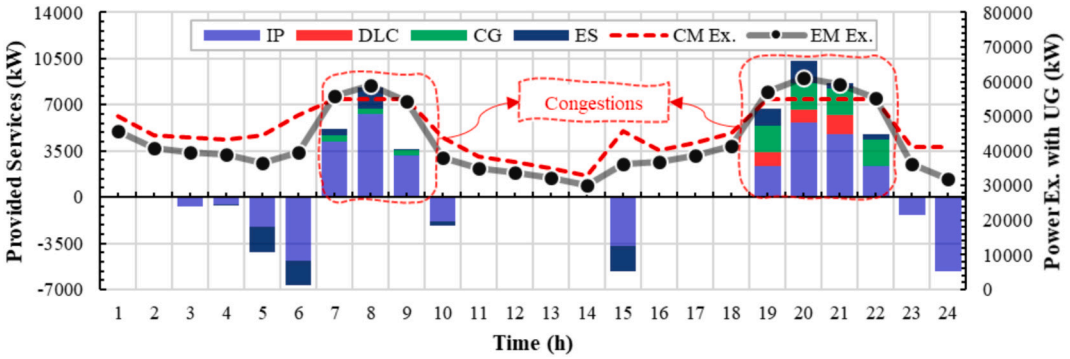


**Fig. 7.** Grid services used for congestion relief in Scenario 3.

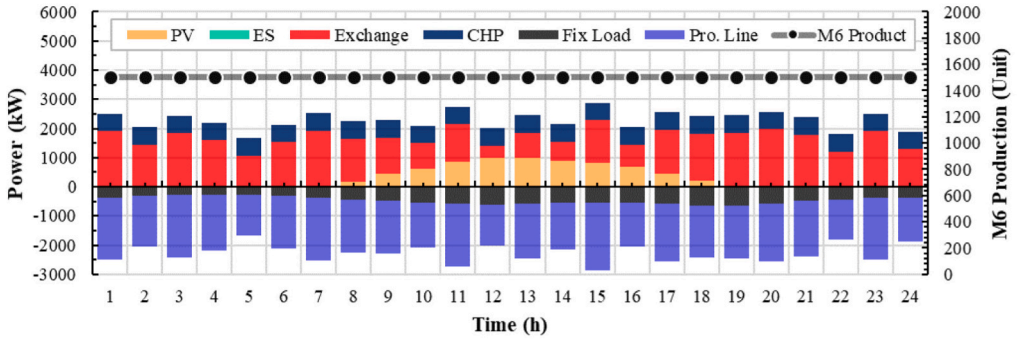


(a) Electrical balance

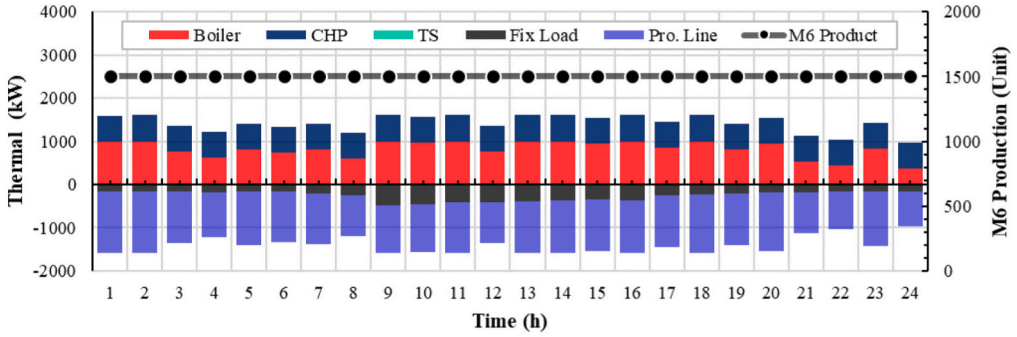


(b) Heat balance

**Fig. 8.** Industrial park schedule in Scenario 2.

heat balances of the industrial park at bus 189 in Scenario 2, while Fig. 9a and b illustrate those corresponding to Scenario 3. A comparison shows that the industrial park in Scenario 3 adjusted its DERs and material production in alignment with CM market signals, providing downward capacity to the DSO during congested periods. Note that the total production level of the M6 product remained constant over the 24-h period, with only temporal adjustments made within permissible limits.

In the fourth scenario, IDCs were activated in the CM market using both load-shifting and service-sharing mechanisms. Table 7 shows that IDCs in Scenario 4 earned a profit of $7117.76 from providing CM services, reducing their net cost by 11.07 %, considering their $2087.91 service-sharing fee and $11,358.79 energy market expense. Moreover, the provision of these services allowed the DSO to completely eliminate the need for DLC contracts for congestion relief, reducing congestion alleviation costs by 27.42 % compared to Scenario 3. Fig. 10 illustrates the capacities employed to alleviate congestion in Scenario 4, confirming that the downward services provided by IDCs fully replaced the DLC contracts, thereby resolving line congestion without any load interruptions. Additionally, the increased availability of downward capacity in Scenario 4 enabled the DSO to rely less on increasing the output of controllable fossil-fueled generators compared to Scenario 3, opting instead for the more cost-effective downward services provided by IDCs. Although the services provided by the industrial parks in Scenario 4 are nearly identical to Scenario 3, as shown in Fig. 10, the cost paid by the DSO to the parks decreased by 63.79 %, as shown in Table 7. This decrease is due to the significant reduction in Locational Marginal Price (LMP) in Scenario 4, as shown in Fig. 11. The higher LMP in Scenario 3 is primarily due to the presence of DLC, which costs twice as much as other services. In the ADMM-based coordination, LMPs are obtained from the dual variables of the nodal balance constraints. Through the ADMM iterations, the DSO and prosumers exchange local schedules and update nodal prices until convergence, at which point the prices represent the marginal cost of power at each node. The decentralized structure,

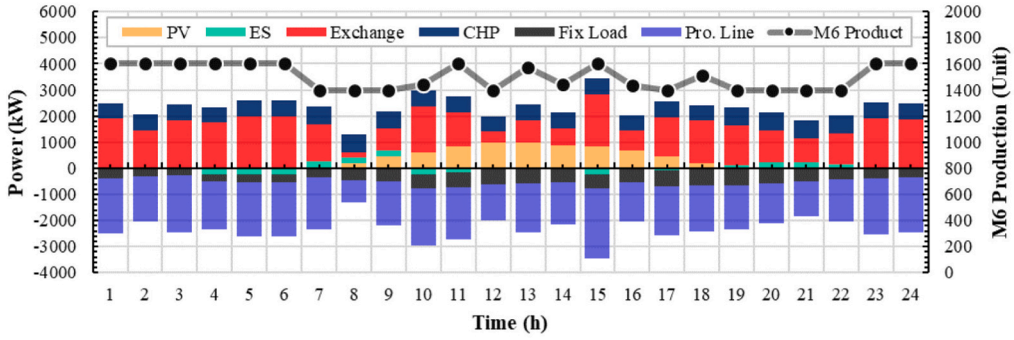


(a) Electrical balance

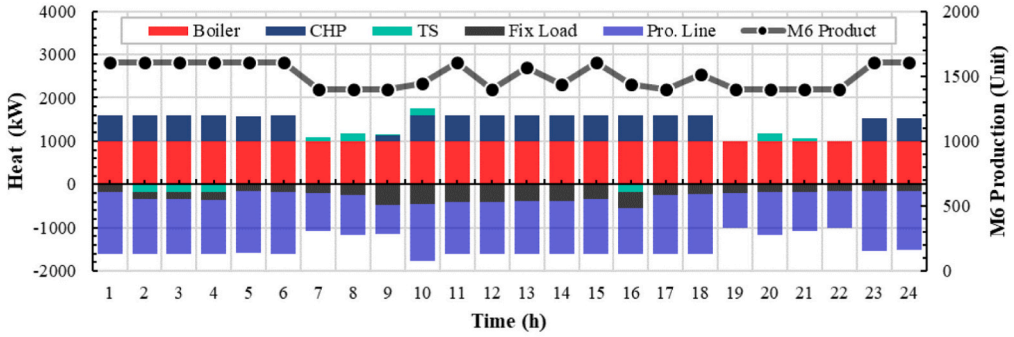


(b) Heat balance

**Fig. 9.** Industrial park schedule in Scenario 3.

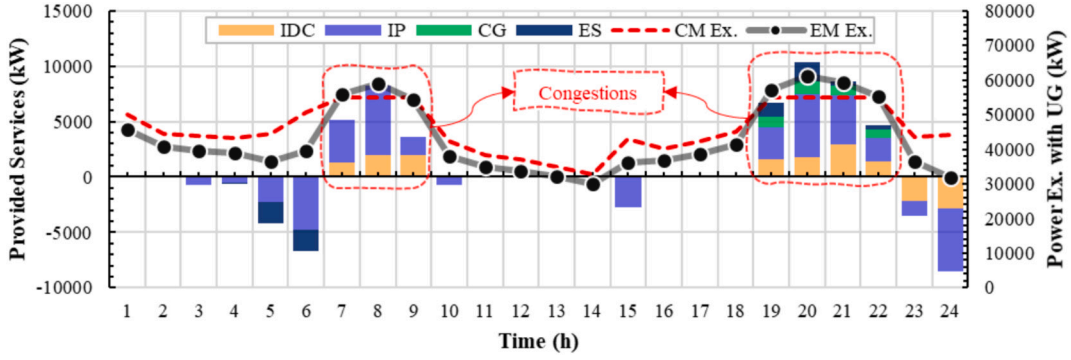


**Fig. 10.** Grid services used for congestion relief in Scenario 4.

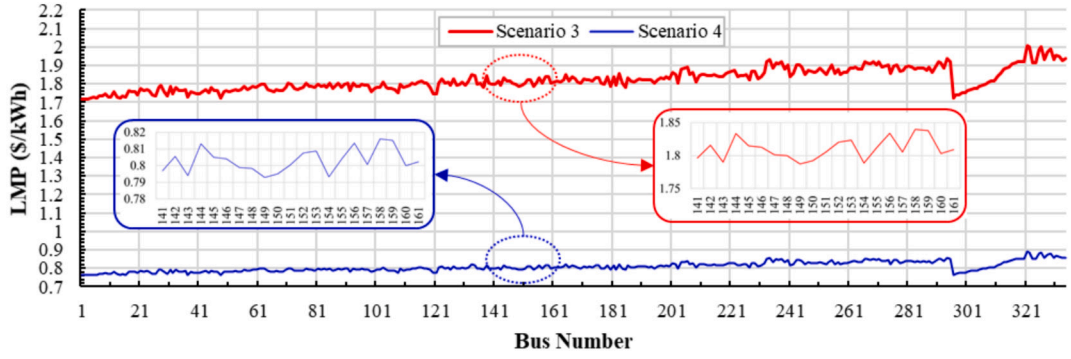


**Fig. 11.** LMP curve obtained for Scenarios 3 & 4.

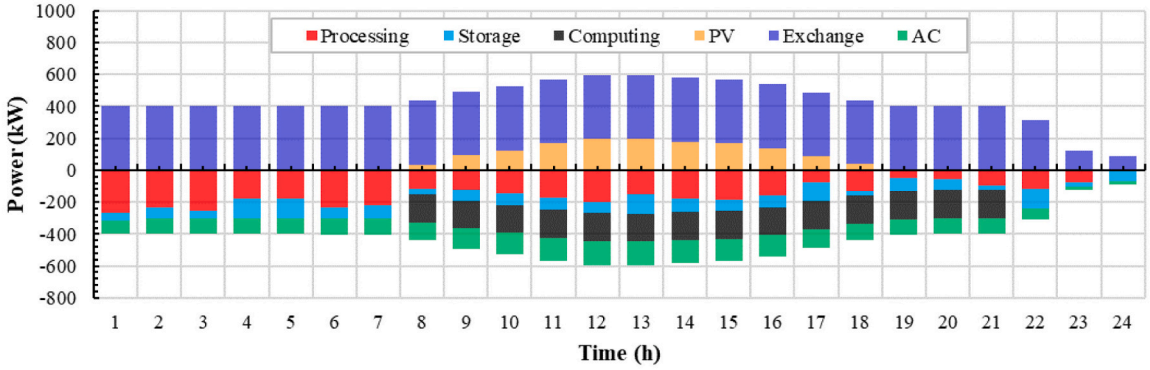


(a) Scenario 3

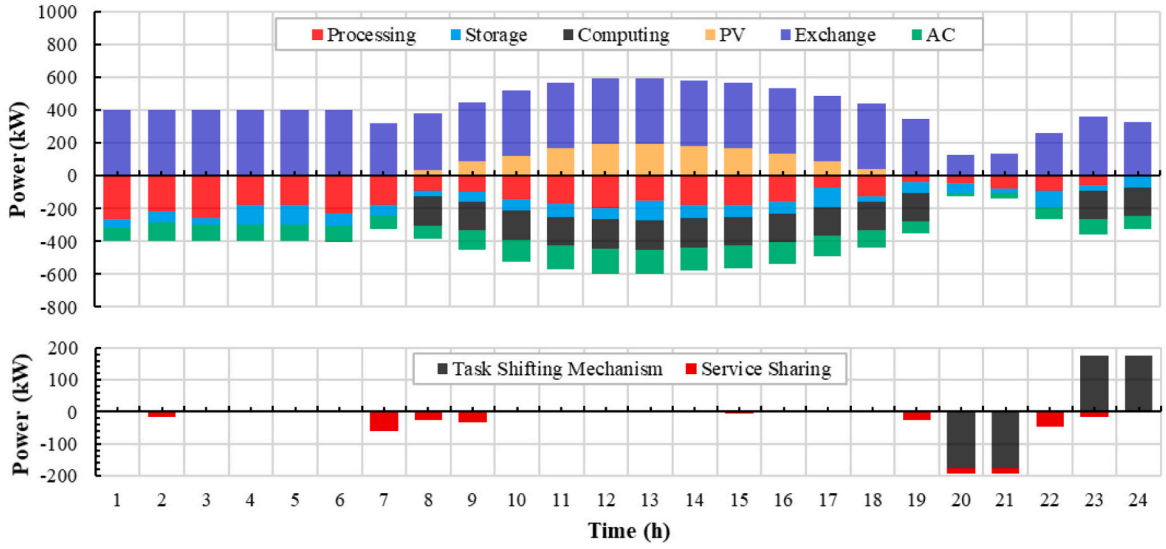


(b) Scenario 4

**Fig. 12.** IDC operational schedule in Scenarios 3 & 4.

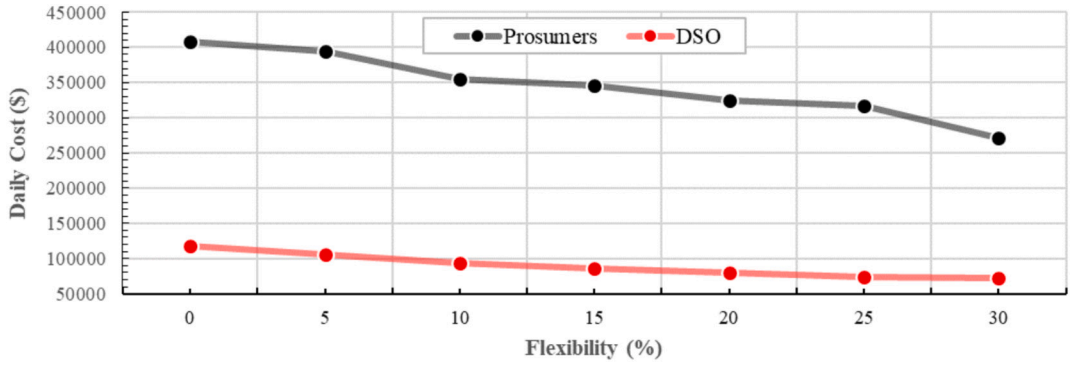


**Fig. 13.** Impact of smart prosumers' participation levels in the CM market on daily costs.

together with nodal pricing and transparent information exchange, ensures efficient and fair market outcomes.

Fig. 12a and b compare the operational schedule for the IDC at bus 222 in Scenarios 3 and 4. It is evident that IDC's participation in the CM market in Scenario 4 significantly altered its workload schedule compared to Scenario 3. Specifically, IDC shifted its interruptible computing services during congestion periods to non-congested hours using the load-shifting mechanism. Additionally, using the service-sharing mechanism, it offloaded a significant portion of its uninterruptible workload, related to processing and storage services, to IDCs in other time zones through the proxy. Specifically, the IDC located in Spain (Zone B) transferred its services to IDCs in Australia (Zone C), earning profit by providing downward services to the DSO while paying the service-sharing fee. Note that time differences between zones prevent overlapping peak periods, enabling IDCs in congested networks within one zone to share services with those in non-congested networks

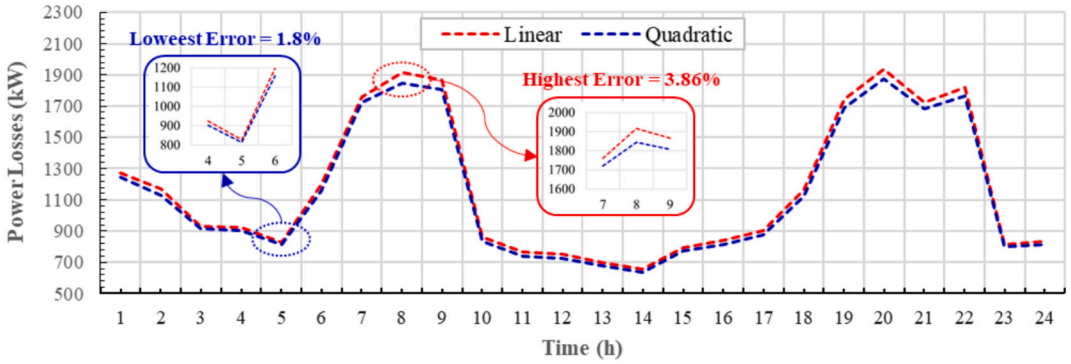


**Fig. 14.** Comparison of power losses from the linearized and quadratic AC power flow models.

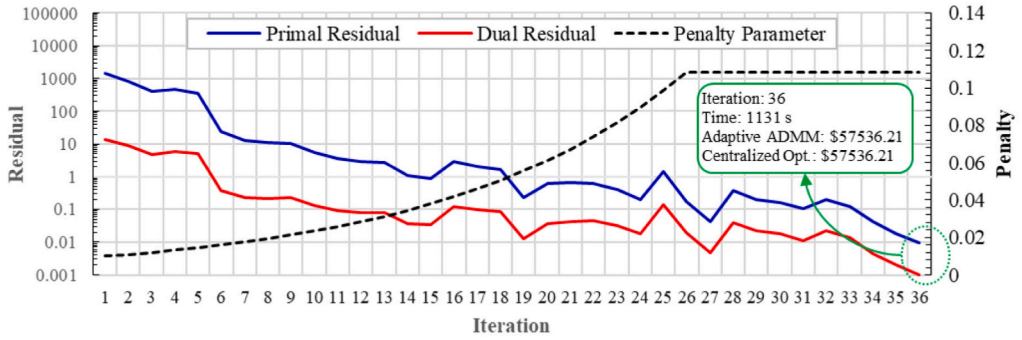


(a) Adaptive ADMM

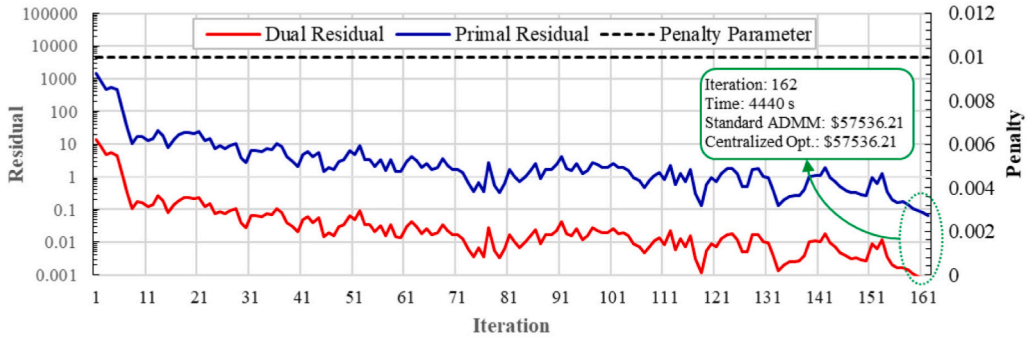


(b) Standard ADMM

**Fig. 15.** Convergence of the proposed and standard versions.

in other zones, effectively delivering grid services.

A sensitivity analysis is conducted to assess the impact of smart prosumers' participation in the CM market on the daily costs of both the DSO and the prosumers. As shown in Fig. 13, seven participation levels are considered, starting from a baseline case without CM service provision up to a scenario where prosumers are allowed to deviate up to 30 % from their scheduled energy quantities in the day-ahead energy market. The results show that increasing participation levels significantly reduces the daily costs for both the DSO and the prosumers. At the 30 % participation level, the DSO's cost decreases by 38.94 %, while the prosumers' aggregate cost decreases by 33.54 % relative to the baseline.

An additional analysis is performed to assess the impact of applying the piecewise linearization technique within the proposed linear AC power flow model. The method is employed to linearize the quadratic terms associated with the active and reactive power components, based on which the power losses are subsequently calculated. As illustrated in Fig. 14, the obtained results are compared with the real losses calculated from the quadratic AC power flow formulation. The piecewise linear approximation is implemented using 11 linear segments, resulting in a low error ranging from 1.8 % to 3.86 % compared to the actual losses. This deviation is negligible, considering the substantial computational advantages of the linearized approach, which enables the power flow model to be embedded within an iterative distributed optimization framework, such as ADMM. In this context, the power flow model is solved at each iteration within the DSO's subproblem, which would be computationally demanding and inefficient if a quadratic power flow formulation were adopted instead.

Finally, Fig. 15a and b illustrate the evolution of the primal and dual residuals, together with the progression of the ADMM penalty parameter in both the adaptive and standard implementations. As shown, both decentralized implementations, the adaptive ADMM and the standard ADMM, converge to the same solution as the centralized optimization, with a value of $57,536.21. Reaching an identical outcome to the centralized benchmark demonstrates that both ADMM versions satisfy

the market-efficiency criterion, ensuring that the decentralized market-clearing process reproduces the socially optimal (centralized) allocation and leads to fair market outcomes for all participating agents. However, the proposed adaptive model achieves convergence 126 iterations earlier, corresponding to a 74.52 % improvement in computational efficiency. This acceleration arises from the dynamic adjustment of the ADMM penalty parameter, which responds to variations in the behavior of market agents. In contrast, the standard approach maintains a fixed penalty parameter throughout the iterations, limiting its adaptability and convergence speed.

## 6. Conclusion

This study presented a distributed optimization mechanism designed to maximize congestion alleviation services provided by industrial parks and IDCs. The mechanism employed a bi-level structure that linked the upper and lower levels through an adaptive ADMM approach, which operated 74.52 % faster than the standard ADMM. This formulation allowed market agents to optimize their operations individually with minimal information exchange. The mechanism was implemented on a 334-bus real-world case study in Spain. The results demonstrated that the system operator was able to fully utilize the cost-effective grid services offered by smart prosumers, leading to a 35.27 % reduction in daily congestion alleviation costs, a lower dependence on fossil-fueled generators, and reduced load shedding associated with DLC contracts. Furthermore, the mechanism enabled industrial parks to optimize material production planning and allowed IDCs to adjust load-shifting and service-sharing strategies in response to DSO requests, resulting in daily cost reductions of 13.68 % and 11.07 %, respectively.

While the proposed mechanism proved highly effective in enhancing congestion management and distributed coordination, certain limitations remain that could guide future improvements, including its reliance on the availability of flexible resources, the accuracy of network and market data, and the computational complexity of large-scale implementations. Future research could explore the deployment of the proposed framework under real-world conditions using advanced digital platforms (e.g., Microsoft Azure), enhance privacy and resilience in real-time coordination against potential cyber and data integrity attacks, and extend the market framework to include commercial and residential participants.

## CRediT authorship contribution statement

**Seyed Amir Mansouri:** Writing – original draft, Supervision, Software, Methodology, Investigation, Conceptualization. **Emad Nematbakhsh:** Resources, Investigation, Data curation. **Andrés Ramos:** Validation, Supervision, Conceptualization. **Jose Pablo Chaves-Avila:** Validation, Project administration, Formal analysis. **Javier García-González:** Validation, Formal analysis. **José A. Aguado:** Supervision, Resources.

## Declaration of competing interest

The authors declare that they have no known competing financial interests or personal relationships that could have appeared to influence the work reported in this paper.

## Acknowledgement

This work was supported by the Strategic Projects Program for Ecological and Digital Transition funded by NextGenerationEU/PRTR through the Spanish Ministry of Science and Innovation/State Research Agency, under reference number TED2021-131365B-C43.

## Data availability

Data will be made available on request.

## References

[1] Hassine L, Quadar N, Ledmaoui Y, Chaibi H, Saadane R, Chehri A, et al. Enhancing smart grid security in smart cities: a review of traditional approaches and emerging technologies. Appl Energy 2025;398:126430. https://doi.org/10.1016/j.apenergy.2025.126430.
[2] Balasubramanian C, Singh Lal Raja, R.. IOT based energy management in smart grid under price based demand response based on hybrid FHO-RERNN approach. Appl Energy 2024;361:122851. https://doi.org/10.1016/j.apenergy.2024.122851.
[3] Mao Y, Lin X, Zhang S, Wang J, Zhong W, Liu B, et al. Optimal scheduling of industrial park integrated energy systems considering dynamics of multiple fluid networks. J Clean Prod 2025;514:145743. https://doi.org/10.1016/j.jclepro.2025.145743.
[4] Zhang Y, Zou B, Jin X, Luo Y, Song M, Ye Y, et al. Mitigating power grid impact from proactive data center workload shifts: a coordinated scheduling strategy integrating synergistic traffic - data - power networks. Appl Energy 2025;377:124697. https://doi.org/10.1016/j.apenergy.2024.124697.
[5] Zhou X, Qi L, Pan N, Hou M, Yang J. Optimization method for load aggregation scheduling in industrial parks considering multiple interests and adjustable load classification. Energy 2025;326:135887. https://doi.org/10.1016/j.energy.2025.135887.
[6] Fan J, Yan R, He Y, Zhang J, Zhao W, Liu M, et al. Stochastic optimization of combined energy and computation task scheduling strategies of hybrid system with multi-energy storage system and data center. Renew Energy 2025;242:122466. https://doi.org/10.1016/j.renene.2025.122466.
[7] Yadav K, Singh M. Dynamic scheduling of electricity demand for decentralized EV charging systems. Sustain Energy, Grids Networks 2024;39:101467. https://doi.org/10.1016/j.segan.2024.101467.
[8] Moradi M, Farzaneh H. Demand response programs in decentralized hybrid local energy markets: evaluating the impact of risk-adjusted behavior of market players and the integration of renewable energy sources, using a novel bi-level optimization framework. Appl Energy 2025;390:125806. https://doi.org/10.1016/j.apenergy.2025.125806.
[9] Asadi Aghajari H, Niknam T, Shasadeghi M, Sharifhosseini SM, Taabodi MH, Sheybani E, et al. Analyzing complexities of integrating renewable energy sources into smart grid: a comprehensive review. Appl Energy 2025;383:125317. https://doi.org/10.1016/j.apenergy.2025.125317.
[10] Kilthau M, Henkel V, Wagner LP, Gehlhoff F, Fay A. A decentralized optimization approach for scalable agent-based energy dispatch and congestion management. Appl Energy 2025;377:124606. https://doi.org/10.1016/j.apenergy.2024.124606.
[11] Singh SK, Singh AK. Adaptive multi-agent federated learning framework for decentralized peer-to-peer energy trading with advanced pricing optimization. Sustain Energy, Grids Networks 2025;43:101787. https://doi.org/10.1016/j.segan.2025.101787.
[12] Fattaheian-Dehkordi S, Rajaei A, Abbaspour A, Fotuhi-Firuzabad M, Lehtonen M. Distributed transactive framework for congestion Management of Multiple-Microgrid Distribution Systems. IEEE Trans Smart Grid 2022;13:1335–46. https://doi.org/10.1109/TSG.2021.3135139.
[13] Zhang W, Xu Y, Tang C. Two-time-scale congestion management scheme for microgrid integrated distribution networks. CSEE J Power Energy Syst 2023;9:1312–25. https://doi.org/10.17775/CSEEJPES.2021.02420.
[14] Talari S, Birk S, Ketter W, Schneiders T. Sequential clearing of network-aware local energy and flexibility Markets in Community-Based Grids. IEEE Trans Smart Grid 2024;15:405–17. https://doi.org/10.1109/TSG.2023.3276024.
[15] Nagpal H, Avramidis I-I, Capitanescu F, Madureira AG. Local energy communities in Service of Sustainability and Grid Flexibility Provision: hierarchical Management of Shared Energy Storage. IEEE Trans Sustain Energy 2022;13:1523–35. https://doi.org/10.1109/TSTE.2022.3157193.
[16] Hu J, Liu X, Shahidehpour M, Xia S. Optimal operation of energy hubs with large-scale distributed energy resources for distribution network congestion management. IEEE Trans Sustain Energy 2021;12:1755–65. https://doi.org/10.1109/TSTE.2021.3064375.
[17] Wei J, Zhang Y, Wang J, Wu L, Zhao P, Jiang Z. Decentralized demand management based on alternating direction method of multipliers algorithm for Industrial Park with CHP units and thermal storage. J Mod Power Syst Clean Energy 2022;10:120–30. https://doi.org/10.35833/MPCE.2020.000623.
[18] Qiu D, Liu D, Gao F, Lu H. Double-layer optimization of Industrial-Park energy system based on discrete hybrid automaton. IEEE Internet Things J 2023;10:7528–36. https://doi.org/10.1109/JIOT.2022.3185173.
[19] Hui H, Bao M, Ding Y, Meinrenken CJ. Incorporating multi-energy industrial parks into power system operations: a high-dimensional flexible region method. IEEE Trans Smart Grid 2024:1. https://doi.org/10.1109/TSG.2024.3426997.
[20] Wei J, Zhang Y, Wang J, Wu L. Distribution LMP-based demand Management in Industrial Park via a bi-level programming approach. IEEE Trans Sustain Energy 2021;12:1695–706. https://doi.org/10.1109/TSTE.2021.3062044.
[21] Dvorkin V. Agent coordination via contextual regression (AgentCONCUR) for data Center flexibility. IEEE Trans Power Syst 2024:1–11. https://doi.org/10.1109/TPWRS.2024.3442954.

[22] Ma J, Yao R, Zhang B, Wang Z, Yan Y. Data-driven flexibility capability Modeling of internet data Center considering task dependency. IEEE Internet Things J 2024; 11:24538–50. https://doi.org/10.1109/JIOT.2024.3395837.
[23] Shi T, Ma H, Chen G, Hartmann S. Auto-scaling containerized applications in geo-distributed clouds. IEEE Trans Serv Comput 2023;16:4261–74. https://doi.org/10.1109/TSC.2023.3317262.
[24] Song J, Zhu P, Zhang Y, Yu G. CloudSimPer: simulating geo-distributed Datacenters powered by renewable energy mix. IEEE Trans Parallel Distrib Syst 2024;35: 531–47. https://doi.org/10.1109/TPDS.2024.3357532.
[25] Wang P, Cao Y, Ding Z, Tang H, Wang X, Cheng M. Stochastic programming for cost optimization in geographically distributed internet data Centers. CSEE J Power Energy Syst 2022;8:1215–32. https://doi.org/10.17775/CSEEJPES.2020.02930.
[26] Mansouri SA, Nematbakhsh E, Ramos A, Ávila JPC, García-González J, Jordehi AR. Bi-level mechanism for decentralized coordination of internet data centers and energy communities in local congestion management markets. IEEE Int. Conf Energy Technol Futur Grids 2023;2023:1–6. https://doi.org/10.1109/ETFG55873.2023.10407758.
[27] Shen F, Lin S, Wei J, Huang S, Wu Q, Shen Y, et al. Distributed dynamic tariff for congestion Management in Distribution Networks Considering Temporal-Spatial Coordination of electric vehicles. IEEE Trans Transp Electrif 2023:1. https://doi.org/10.1109/TTE.2023.3332892.
[28] Fattaheian-Dehkordi S, Tavakkoli M, Abbaspour A, Fotuhi-Firuzabad M, Lehtonen M. An incentive-based mechanism to alleviate active power congestion in a multi-agent distribution system. IEEE Trans Smart Grid 2021;12:1978–88. https://doi.org/10.1109/TSG.2020.3037560.
[29] Mansouri SA, Nematbakhsh E, Ramos A, Tostado-Véliz M, Aguado JA, Aghaei J. A robust ADMM-enabled optimization framework for decentralized coordination of microgrids. IEEE Trans Ind Informatics 2024:1–10. https://doi.org/10.1109/TII.2024.3478274.
[30] Tofighi-Milani M, Fattaheian-Dehkordi S, Fotuhi-Firuzabad M, Lehtonen M. Decentralized active power Management in Multi-Agent Distribution Systems Considering Congestion Issue. IEEE Trans Smart Grid 2022;13:3582–93. https://doi.org/10.1109/TSG.2022.3172757.
[31] Khan OGM, Youssef A, Salama M, El-Saadany E. Robust multi-objective congestion Management in Distribution Network. IEEE Trans Power Syst 2023;38:3568–79. https://doi.org/10.1109/TPWRS.2022.3200838.
[32] OptiREC: Local markets for energy communities: designing efficient markets and assessing the integration from the electricity system perspective. https://www.iit.comillas.edu/publicacion/proyecto/en/MCI_OptiREC/OptiREC._Mercados_locales_para_comunidades_energéticas:_diseño_de_mercados_eficientes_y_evaluación_de_la_integración_desde_la_perspectiva_del_sistema_eléctrico; 2022.
[33] Mansouri SA, Nematbakhsh E, Jordehi AR, Marzband M, Tostado-Véliz M, Jurado F. An interval-based nested optimization framework for deriving flexibility from smart buildings and electric vehicle fleets in the TSO-DSO coordination. Appl Energy 2023;341:121062. https://doi.org/10.1016/j.apenergy.2023.121062.
[34] Mansouri SA, Ramos A, Ávila JPC, García-González J, Aguado JA. A DSO-driven privacy-preserving mechanism for managing power exchanges in Australian networks. IEEE Trans Ind Informatics 2025:1–11. https://doi.org/10.1109/TII.2025.3586048.
[35] Input data for OptiREC5. https://pascua.iit.comillas.edu/aramos/Simulation_Input_Data.xlsx; 2025.